U.S. DEPARTMENT OF ENERGY | Office of Science

DOE/SC-ARM-16-023

Enhanced Soundings for Local Coupling Studies Field Campaign Report

CR Ferguson
JA Santanello
P Gentine

April 2016

ARM
CLIMATE RESEARCH FACILITY

DISCLAIMER

DOE/SC-ARM-16-023

Enhanced Soundings for Local Coupling Studies Field Campaign Report

CR Ferguson, University at Albany, State University of New York
JA Santanello, National Aeronautics and Space Administration
P Gentine, Columbia University
Principal Investigators

April 2016

Work supported by the U.S. Department of Energy,
Office of Science, Office of Biological and Environmental Research

Executive Summary

This document presents initial analyses of the enhanced radiosonde observations obtained during the U.S. Department of Energy (DOE) Atmospheric Radiation Measurement (ARM) Climate Research Facility Enhanced Soundings for Local Coupling Studies Field Campaign (ESLCS), which took place at the ARM Southern Great Plains (SGP) Central Facility (CF) from June 15 to August 31, 2015. During ESLCS, routine 4-times-daily radiosonde measurements at the ARM-SGP CF were augmented on 12 days (June 18 and 29; July 11, 14, 19, and 26; August 15, 16, 21, 25, 26, and 27) with daytime 1-hourly radiosondes and 10-minute 'trailer' radiosondes every 3 hours. These 12 intensive operational period (IOP) days were selected on the basis of prior-day qualitative forecasts of potential land-atmosphere coupling strength. The campaign captured 2 dry soil convection advantage days (June 29 and July 14) and 10 atmospherically controlled days. Other noteworthy IOP events include: 2 soil dry-down sequences (July 11-14-19 and August 21-25-26), a 2-day clear-sky case (August 15-16), and the passing of Tropical Storm Bill (June 18). To date, the ESLCS data set constitutes the highest-temporal-resolution sampling of the evolution of the daytime planetary boundary layer (PBL) using radiosondes at the ARM-SGP. The data set is expected to contribute to: 1) improved understanding and modeling of the diurnal evolution of the PBL, particularly with regard to the role of local soil wetness, and (2) new insights into the appropriateness of current ARM-SGP CF thermodynamic sampling strategies.

This document provides results from the following 4 tasks: 1) characterization of IOP days according to convection and land-atmosphere coupling relevant parameters, 2) estimation of PBL height and intercomparison with official ARM PBL-height value-added product (VAP) estimates, 3) evaluation of daytime variability in low-level atmospheric humidity and instability, and 4) quantification of uncertainty in radiosonde characterization of the mean thermodynamic structure. Based on 48 pairs of daytime 10-minute-lagged radiosondes and uncertainty in the warm season 0-300 hPa above-ground-level (AGL) layer radiosonde temperature, relative humidity and specific humidity were estimated at 0.24-0.29 K, 2.2-3.4% and 0.36-0.41 g kg^{-1}, respectively. During ESLCS, there were instances in which the 10-minute-lagged pair differed by 1 K for a single 10-hPa layer and by 2 K and 30% for a 100-hPa layer in the lower atmosphere. The mean absolute difference in daytime low-level humidity index and convective triggering potential relative to 1130 UTC (0530 local standard time [LST]) estimates were found to be 3.7-7.2 K and 94-195 J kg^{-1}, respectively. Daytime PBL evolution was well captured by the campaign; however, substantial spread (up to 3000 m) among competing estimates of PBL height serves to highlight the need for a single community best-practice recommendation to foster intercomparison studies. Several other immediate research opportunities are identified, including a call for more careful accounting of the roles of frontal systems and other large-scale atmospheric disturbances in land-atmosphere coupling.

Acronyms and Abbreviations

AGL	above ground level
AERI	Atmospheric Emitted Radiance Interferometer
AIRS	Atmospheric Infrared Sounder, a scanning instrument aboard Aqua
AMSR-E	Advanced Microwave Scanning Radiometer–Earth Observing System, an instrument aboard Aqua that measures polarized brightness temperatures
Aqua	a multi-national NASA water research satellite
ARM	Atmospheric Radiation Measurement Climate Research Facility
As-PECAN	ARM Support for the Plains Elevated Convection at Night field campaign
Aura	a multi-national NASA satellite studying the ozone layer, air quality, and climate
CALIPSO	a joint NASA-CNES environmental research satellite
CBL	convection boundary layer
CDT	Central Daylight Time
CERES	Clouds and the Earth's Radiant Energy System, a cloud imaging instrument aboard Aqua and Terra
CF	Central Facility
CloudSat	a NASA Earth-observation satellite
CNES	Centre National d'Etudes Spatiales
CTP-HI	convective triggering potential-humidity index
DMF	ARM Data Management Facility
DOE	U.S. Department of Energy
DTR	diurnal temperature range
EF	evaporation fraction
ESLCS	Enhanced Soundings for Local Coupling Studies field campaign
GCOM	Global Change Observation Mission, a series of Japanese satellites
GEWEX	Global Energy and Water Cycle Exchanges
GLACE	Global Land Atmosphere Coupling Experiment
IASI	Infrared Atmospheric Sounding Interferometer, aboard MetOp-A/B
IOP	intensive operational period
LCL	lifting condensation level
LFC	level of free convection
LoCo	Local Coupling
LLJ	low-level jet
lst	local standard time
MAD	Mean Absolute Difference
MetOp-A/B	European polar orbiting meteorological satellites that carry IASI
MODIS	Moderate Resolution Imaging Spectroradiometer, aboard Aqua and Terra

NARR	North American Regional Reanalysis
NASA	National Aeronautics and Space Administration
NCEP	National Centers for Environmental Prediction
NLDAS-2	North American Land Data Assimilation System project, Phase 2
NLLJ	nocturnal low-level jet
NSSL	National Severe Storms Laboratory
NWS	National Weather Service
PARASOL	Polarization and Anisotropy of Reflectances for Atmospheric Sciences coupled with Observations from a Lidar, a French Earth-observation satellite
PBL	planetary boundary layer
PBLh	planetary boundary layer height
PBLh VAP	ARM's Planetary Boundary Layer Height Value-Added Product
RH	relative humidity
SGP	Southern Great Plains, an ARM megasite
SH	surface sensible heat flux
SSMRS	Scintillometry and Soil Moisture Remote Sensing field campaign
Terra	a multi-national NASA research satellite monitoring Earth's environment and changes in its climate
THWAPS	temperature, humidity, wind, and pressure system
UTC	Coordinated Universal Time
VAP	Value-Added Product
WCRP	World Climate Research Programme
WRF	Weather Research and Forecasting

Contents

Figures

Tables

1.0 Introduction

1.1 Purpose and Scope

The planetary boundary layer (PBL) is the region in the atmosphere where the influence of local terrain and terrestrial processes and anomalies on large-scale atmospheric processes is felt, and the majority of atmospheric water vapor, heat, momentum, carbon, aerosols, and chemical constituents are transported. Turbulence in the PBL and its coupling with free-tropospheric conditions controls convective initiation, cloud coverage, and precipitation distribution and intensity. Observations show that, depending on the structure of the PBL, the following phenomena may be suppressed or supported: heat waves, severe thunderstorms, and tornadoes; prolonged wetness and drought; and dispersion of environmental (e.g., dust and smoke) and anthropogenic (e.g., pollution) emissions. In a 2012 survey of international experts in land-atmosphere interaction conducted by the Local Coupling (LoCo) (Santanello et al. 2011) working group of the World Climate Research Programme's (WCRP) Global Energy and Water Cycle Exchanges (GEWEX) project, the lack of high-temporal-resolution soundings (i.e., 1-hourly) and associated uncertainty estimates was identified as the prominent barrier to improved understanding and modeling of the daytime evolution of the PBL (Ferguson et al. 2012). An improved representation of the PBL is a prerequisite for next-generation model simulations of clouds and precipitation as well as extreme events in weather forecast and climate models.

The Enhanced Soundings for Local Coupling Studies Campaign (EXLCS) (Ferguson et al. 2014) was designed to:

1. Contribute to the improved understanding, observation, and modeling of the diurnal evolution of the PBL, and in particular, the role of the land surface in this process.

2. Identify the optimal time(s), measurement(s), and sampling frequency for characterizing daily land-atmosphere coupling strength over the southern Great Plains.

ESLCS was carried out at the ARM Facility's Southern Great Plains (SGP) site, the largest and most extensively instrumented research field site in the world. The SGP was designated in the GEWEX Global Land Atmosphere Coupling Experiment (GLACE) (Guo et al. 2006, Koster et al. 2004, Koster et al. 2006) as a land-atmosphere coupling 'hotspot', or a region where realistic land states (namely, soil moisture) can improve temperature and precipitation predictability on sub-seasonal timescales.

During the ESLCS campaign, routine 4x daily (0530, 1130, 1730, and 2330 UTC) radiosondes at the ARM-SGP Central Facility (CF) (36.6°N, 97.5°W) were augmented on 12 intensive operational period (IOP) days (6/18, 6/29, 7/11, 7/14, 7/19, 7/26, 8/15, 8/16, 8/21, 8/25, 8/26, and 8/27) by daytime (1130-2330 UTC) 1-hourly radiosondes with 10-minute 'trailer' radiosondes every 3-hours (see Fig. 1 for full schedule). The campaign radiosonde frequency was designed to fully capture the daytime evolution of the PBL. The purpose of the 10-minute 'trailer' radiosondes was to enable quantification of atmospheric temporal variability, or from another perspective, uncertainty in a given radiosonde's characterization of the mean thermodynamic structure. Also, 'trailer' radiosondes would provide a means to determine whether one of the 10-minute-lagged radiosondes had been launched within a roll updraft (Weckwerth et al. 1996, Bennett et al. 2010). On average, a radiosonde ascends to 300 hPa above ground level (AGL) at a point 4 km downwind from its launch site within 10 minutes of launch.

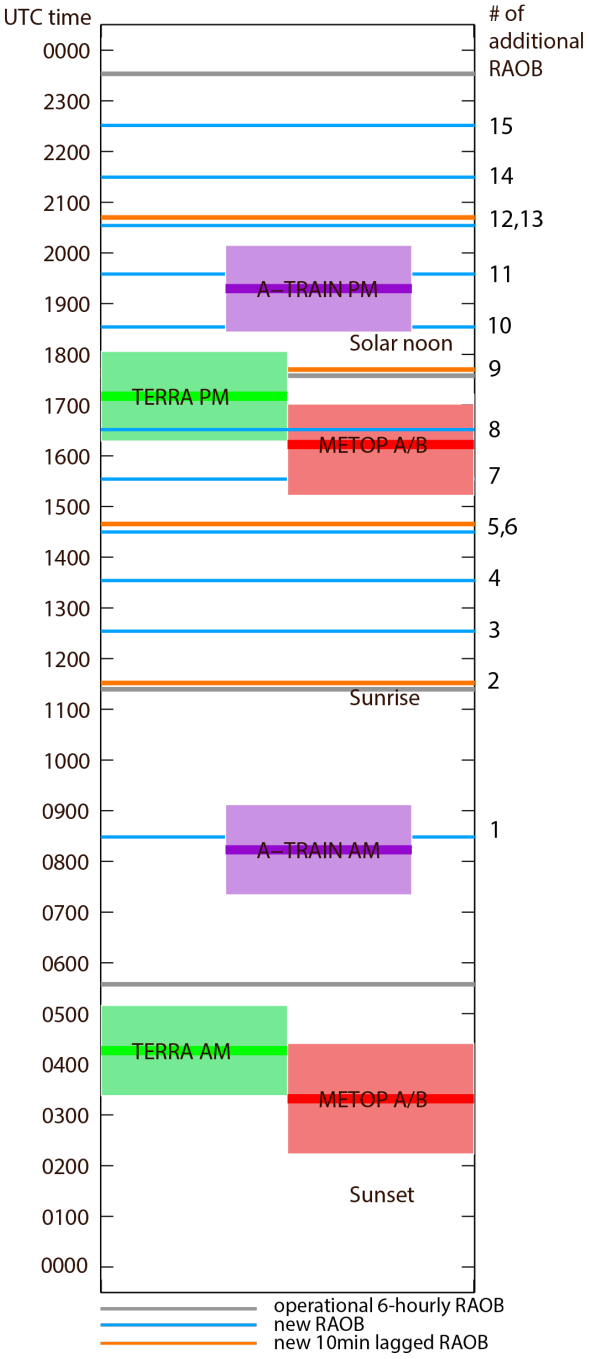

Figure 1. July 2015 overpass times at ARM-SGP for several space-borne platforms superimposed on the ESLCS campaign launch schedule (in UTC: 0530, 0830, 1130, 1140, 1230, 1330, 1430, 1440, 1530, 1630, 1730, 1740, 1830, 1930, 2030, 2040, 2130, 2230, and 2330). The A-Train consists of GCOM-W1, Aqua, CloudSat, CALIPSO, PARASOL, and Aura. Aqua carries AIRS, CERES, and AMSR-E; Terra carries CERES and MODIS; MetOp-A/B both carry IASI (see Acronyms and Abbreviations for definitions).

Overall, the ESLCS campaign was conducted in the context of the convective triggering potential-humidity index (CTP-HI) land-atmosphere coupling regime framework (Findell and Eltahir 2003a). CTP and HI are measures of the early-morning atmospheric instability and low-level moisture in the portion of the vertical profile that is almost always incorporated into the growing daytime PBL. Specifically, CTP (J kg^{-1}) is defined as the integral of the area between the temperature sounding profile, T_{env} (K), and a moist adiabat, T_{parcel} (K), raised from the observed temperature and humidity 100 hPa (approx.1 km) AGL to a level 300 hPa (approx. 3 km) AGL. HI is defined as the sum of the dewpoint depressions at 50 and 150 hPa pressure AGL. The CTP-HI framework defines four regimes: a dry-advantage regime for which convective triggering is preferentially favored over drier than average soils, a wet-advantage regime for which convective triggering is preferentially favored over wetter than average soils, a transition regime for which soil wetness can have varied effect on convective triggering, and an atmospherically-controlled regime for which the surface wetness does not play a role in convective triggering because either the atmosphere is so dry and/or stable that deep convection is unlikely, or the atmosphere is so humid and unstable that convection is very likely.

The original Findell and Eltahir (2003b) implementation was developed using 1130 UTC (sunrise) radiosondes. However, atmospheric soundings from the Atmospheric Infrared Sounder (AIRS) onboard NASA Aqua are conveniently available for the SGP at approximately 0830 UTC (descending overpass) for the period from 2002-present. For the purpose of assessing the appropriateness of 0830 UTC CTP and HI estimates relative to the framework's intended inputs of 1130 UTC CTP and HI (Ferguson and Wood

2011, Findell and Eltahir 2003b), an 0830 UTC radiosonde was added to the ESLCS launch schedule (Fig. 1).

The ESLCS data set constitutes the highest-ever temporal resolution sampling of the evolution of the daytime PBL using radiosondes at the SGP. Two other ARM-supported campaigns overlapped with ESLCS: 1) the ARM Support for the Plains Elevated Convection at Night (As-PECAN) campaign (Turner et al., 2014), which provided for 3-hourly radiosonde launches (2030, 2330, 0230, 0530, 0830, and 1130 UTC) at the CF over the course of PECAN (Geerts et al. 2013) (1 June to 15 July); and 2) the Scintillometry and Soil Moisture Remote Sensing campaign (SSMRS) (Hendrickx and Kleissl 2015), which provided temporally continuous sensible heat flux measurements over four, approximately 500-m, homogeneous scintillometer transects at the ARM-SGP CF.

The augmentation of the ARM-SGP CF operational suite of instruments with hourly daytime radiosondes was anticipated to lead to new insights into the appropriateness of current ARM-SGP thermodynamic sampling strategies. In helping to address what ARM could do to better observe land-atmosphere coupling and to better support the evaluation and refinement of coupled models, ESLCS was directly responsive to two of ARM's priorities for 2012-2017: 1) "*optimize the collection and reporting of observations in ways that best address the collective needs of [atmospheric and modeling] communities*" and 2) "*further expand the capabilities of the sites, specifically the Southern Great Plains site, to develop testbeds for better understanding of the coupling of the land, ecosystem, and atmospheric interactions*" (DOE-BER 2012).

A first look at the ESLCS data reveals that the campaign successfully sampled a wide range of PBL conditions, spanning shallow to deep PBL growth and including some 'textbook' PBL growth days characterized with incremental growth and a well-defined PBL top. The nocturnal residual layers are clearly distinguishable on some days, as well. Other days feature more complex PBL profiles, which will require extra skill in analysis and interpretation.

1.2 Approach

Our objective from the outset of the campaign was to capture one 3-day (or longer) event each for wet-advantage (expected in June-July) and dry-advantage land-atmosphere interaction coupling regimes (expected in July-August). Based on analysis of the 36-year (1979-2014) North American Regional Reanalysis (NARR) (Mesinger et al. 2006) data by PI Ferguson, we knew that typical wet-advantage events occur when the Great Plains low-level jet (LLJ) is not active in the preceding 24-hours. Conversely, typical dry-advantage events occur when the LLJ is active. Additionally, low-level winds (850hPa and lower) are historically southerly for wet-advantage days and southwesterly for dry-advantage days. In both cases (wet- and dry-advantage), morning 10-m winds tend to be less than 4.5 m s^{-1} (10 mph), morning cloud fraction tends to be less than 40%, and there is no significant morning rainfall. Finally, the role of the land will be most readily distinguishable under conditions of weak atmospheric synoptic forcing, for example, in the absence of a frontal system or tropical storm. We used these known characteristics of wet- and dry-advantage coupling events to screen weather forecasts for candidate IOP days. In the process of targeting these multi-day events, we expected to accumulate up to 6 isolated "false-start" days, due to conditions being other than forecasted or simply deteriorating (in the context of land-atmosphere coupling strength) on Day 1. We were also encouraged by the ARM Facility to capture unique meteorological events if the opportunity presented itself.

In general, we relied on the following forecast sources to inform our IOP selections: National Weather Service (NWS) 5-day forecasts for Lamont, Oklahoma (http://www.weather.gov/); NWS forecast discussions from the Tulsa, Oklahoma (http://kamala.cod.edu/ok/latest.fxus64.KTSA.html) and Oklahoma City, Oklahoma (http://kamala.cod.edu/ok/latest.fxus64.KOUN.html) offices; long-range multi-model guidance from the National Centers for Environmental Prediction (NCEP) Central Operations (http://mag.ncep.noaa.gov/model-guidance-model-area.php?group=Model%20Guidance&model=gfs&area=namer&ps=area#); National Severe Storms Laboratory (NSSL) Weather Research and Forecasting (WRF) 0-36hr forecasts (http://wrf.nssl.noaa.gov//); as well as the 10-day weather forecast for Lamont, Oklahoma from Weather Underground (www.wunderground.com). However, during PECAN, we did consult that campaign's daily weather forecast briefing.

2.0 Notable Events

The 18 June IOP captured the passing of Tropical Storm Bill (NCEP 2015, NHC 2015). The heaviest rainfall fell in south-central Oklahoma between the evening of 17 June and morning of 18 June. Figure 2(a) shows the 15 June-19 June rainfall totals (TWC 2015). Evidence of the storm's track persists in the 90-day precipitation totals for the period ending 1 September. (Fig 2b; http://www.mesonet.org/index.php/weather/category/rainfall). The passing of Tropical Storm Bill capped off an unusually wet spring season for the region and, in fact, the typical August dry-down we expected never materialized (Fig. 2c). Noteworthy weather events are well documented in the Oklahoma Climatological Survey's monthly climate summaries (McManus et al. 2015).

3.0 Lessons Learned

After As-PECAN concluded on 15 July, there was a misunderstanding among ARM staff regarding ESLCS expectations. Six 0830 UTC radiosonde launches were inadvertently omitted on 7/19, 7/26, 8/21, 8/25, 8/26, and 8/27. Recognition of this problem was delayed due to the fact that the full set of campaign radiosonde data was not being stored together in one place. During the campaign, 4 ground receivers (C1, S1-3) were in use with the data for each unit being filed in different ARM archive locations. On 26 July, it was discovered that the S3 unit had not been transmitting data to the ARM Data Management Facility (DMF); up until this date the data were only being saved locally at SGP-ARM. If SGP-ARM had provided launch confirmations at the end of each IOP day, then likely fewer radiosondes would have been missed.

The SGP-ARM technicians held us to a 21-hour (0640 Central Daylight Time [CDT] Day-1) advance notice policy for all IOP days. We learned that full vertical resolution weather forecasts that resolve low-level atmospheric humidity and stability are not always available and that their accuracy for 24-36 hours and the accuracy of common surface meteorology forecasts for 24-hours may not be sufficient for forecasting the potential land surface influence. In particular, we used the NSSL's 36-hour WRF forecasts (http://wrf.nssl.noaa.gov//), which are initialized at 0000 UTC daily. Accordingly, at ~1200 UTC Day-1 when the IOP determination needed to be made, only the NSSL forecast from 0000 UTC Day-1 through

1200 UTC Day 1 was available. In the future, without the aid of an in-house WRF simulation, we suggest a 9-12 hour advanced notice policy, if possible.

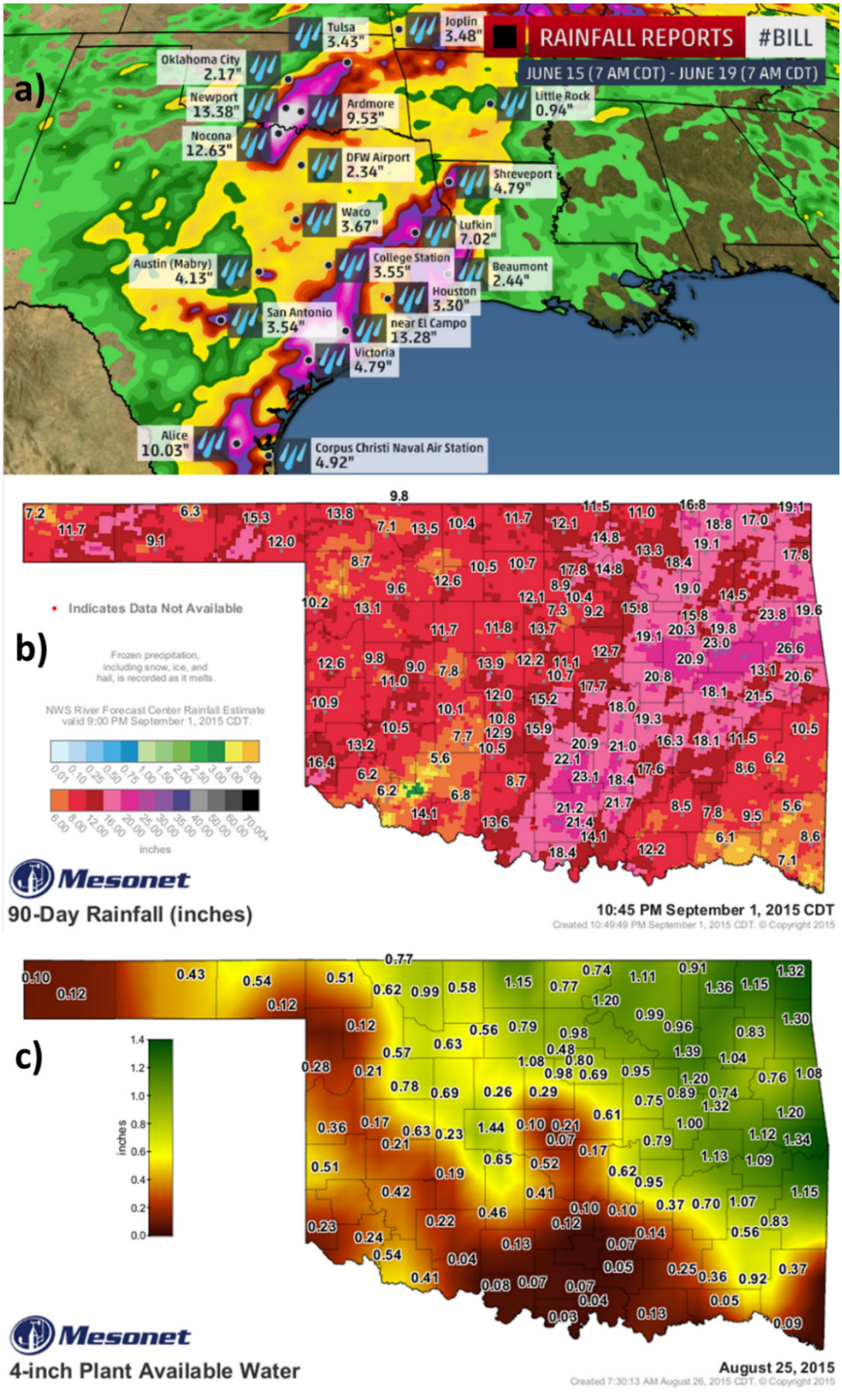

Figure 2. (a) Tropical Storm Bill rainfall totals in inches. (b) Oklahoma Mesonet 90-day rainfall map for the period preceding September 1, 2015. (c) Oklahoma Mesonet 4-inch plant available soil water on August 25, 2015.

4.0 Results

The ESLCS campaign consisted of 2 IOP days in June, 4 IOP days in July, and 6 IOP days in August (Table 1). Two soil moisture dry-down sequences were captured: July 11-14-19 and August 21-25-26. The nocturnal LLJ was active—to varying degrees—on 7 IOP days: 29 June, 11 July, 14 July, 19 July, 26 July, and 15-16 August. The LLJ was weakest on 15-16 August, which comprised an ideal 2-day clear-sky case. In fact, the campaign's largest diurnal temperature range (19.0 °C) was observed on 16 August. Tropical Storm Bill generated precipitation for most of the day (0700-2300 UTC) on 18 June. For the other 5 IOP days when SGP domain-average daily (0000-2359 LST) precipitation exceeded 1 mm, precipitation was typically confined to the morning hours. On 29 June, there were periods of precipitation from 0800-1400 UTC. On 14 July, there were periods of precipitation from 0800-1500 UTC. On 19 July, there were periods of precipitation from 0900-1100 UTC. On 21 August, there were periods of precipitation between 0700-1500 UTC. And on 27 August, there were periods of precipitation between 1100-1800 UTC.

The daily CTP-HI regime classifications were derived from NARR data for the SGP domain (34.35°-38.85°N, 95.25°-99.75°W) following the approach of Roundy et al. (2013). The SGP domain was classified as atmospherically controlled, unless all constituent grid cells were classified either wet- or dry-advantage. The campaign captured 0 of 3 wet-advantage coupling days (6/15, 6/16, and 7/9), 2 of 11 dry-advantage regime days (6/29-7/1, 7/13-7/15, 7/24-7/25, 8/3, 8/7, and 8/31) and 10 of 64 atmospherically controlled regime days (all remaining dates) during the 78-day period from June 15-August 31. June 29 was the first day of a 3-day dry-advantage event. July 14 was the second day of a 3-day dry-advantage event.

Table 1. Convection and land-atmosphere coupling relevant attributes for each of the 12 ESLCS IOP days.

	SGP-ARM CF THWAPS			NLDAS2; SGP Areal Ave. (34.35°-38.85°N, 95.25°-99.75°W)				SGP-ARM CF ESLCS RAOB								
								0530/1730	1130			2030				
2015 ESLCS IOP Date	T_{min} (°C)	T_{max} (°C)	DTR (°C)	Noah 1200 UTC SM_{0-10} (kg m^{-2})	Noah 1800 UTC SH (W m^{-2})	Noah 1800 UTC EF ()	0000-2359 LST *P* (mm)	NLLJ	1130 UTC CTP (J kg^{-1})	1130 UTC HI (K)	1130 UTC 850-700 hPa dT/dz (K km^{-1})	2030 UTC LCL (km)	2030 UTC LFC (km)	2030 UTC q_{PBL} (g kg^{-1})	2030 UTC PBLh (km)	Max. PBLh (UTC time)
18-Jun	21.0	29.8	8.8	28.7	155.3	0.65	10.4	0.0	-61	3.5	-4.8	1.3	3.5	13.2	1.2	2.4 (1931)
29-Jun	21.1	35.6	14.5	23.0	206.3	0.58	1.8	21.0	354	25.3	-8.8	2.9	4.9	8.6	2.7	2.9 (1829)
11-Jul	21.5	33.1	11.6	26.8	204.3	0.63	0.1	15.1	239	11.1	-5.8	1.5	3.1	13.3	2.2	2.5 (1550)
14-Jul	23.6	36.3	12.7	25.0	212.7	0.59	1.5	29.5	190	19.8	-7.9	1.4	2.5	18.9	1.3	1.3 (2027)
19-Jul	23.7	37.4	13.7	23.0	236.7	0.56	1.4	15.7	186	16.4	-5.2	2.2	3.8	12.3	2.7	2.8 (1229)
26-Jul	24.3	35.2	10.9	24.0	215.2	0.59	0.8	15.1	165	22.1	-5.8	2.2	4.1	12.5	1.3	2.1 (1733)
15-Aug	17.5	33.9	16.4	21.4	236.4	0.54	0.0	7.6	-8	28.3	-4.3	2.4	n/a	9.5	1.4	1.8 (2230)
16-Aug	15.8	34.8	19.0	20.8	237.0	0.54	0.0	7.5	26	36.9	-6.5	2.3	n/a	10.0	1.8	2.2 (2328)
21-Aug	17.5	29.1	11.6	23.5	213.7	0.54	2.6	0.0	112	3.7	-6.0	0.7	3.4	15.2	0.9	2.9 (1428)
25-Aug	13.4	30.5	17.1	23.0	215.1	0.56	0.0	0.0	-141	37.3	-5.2	2.1	n/a	8.6	1.0	1.0 (2028)
26-Aug	19.0	34.0	15.0	22.3	213.6	0.55	0.0	0.0	159	5.7	-5.8	1.5	3.0	14.5	2.1	2.1 (2030)
27-Aug	20.1	30.6	10.5	22.0	186.1	0.57	3.4	0.0	374	21.7	-8.0	1.7	5.3	12.0	0.6	2.3 (1629)

During ESLCS, we observed that some days were classified as being in land-atmosphere coupling (i.e., wet- or dry-advantage) by the CTP-HI framework, when in actuality we knew from additional weather observations that significant mid- and/or upper-level disturbances were ongoing and likely acting to limit

any potential role of the land. Our attention to weather forecasting discussions sensitized us to the surprisingly frequent occurrence of mid-to-upper-level disturbances over the SGP during the ESLCS period. In this context we realized the need for additional studies to better understand the overlapping roles of land-atmosphere interactions and mesoscale phenomena.

In Table 1, each IOP day is characterized by several convection and land-atmosphere coupling relevant attributes, inspired by Song et al. (2016; their Fig. 6). The IOP day attributes were derived from three sources: 1) 5-minute SGP-ARM temperature, humidity, wind, and pressure system (THWAPS) measurements, 2) 1-hourly and 0.125° meteorological forcing and Noah v2.8 (Ek et al. 2003) output from Phase 2 of the North American Land Data Assimilation System project (NLDAS-2) (Xia et al. 2012a, Xia et al. 2012b), and 3) ESLCS radiosondes. The attribute table includes: minimum daily 2-m air temperature (T_{min}), maximum daily 2-m air temperature (T_{max}), diurnal 2-m air temperature range (DTR), 1200 UTC 0-10 cm soil moisture ($SM_{0\text{-}10}$), 1800 UTC surface sensible heat flux (SH), 1800 UTC surface evaporative fraction (EF), 0000-2359 LST SGP domain-averaged precipitation (P), nocturnal LLJ (NLLJ) index (Rife et al. 2010), 1130 UTC CTP, 1130 UTC HI, 1130 UTC 850-700 hPa lapse rate (Frye and Mote 2010), 2030 UTC lifting condensation level (LCL), 2030 UTC level of free convection (LFC), 2030 UTC PBL average specific humidity (q_{PBL}), 2030 UTC PBL height (PBLh), and the daily maximum PBLh. For each column, the minimum and maximum values are highlighted in blue and red, respectively. The PBLh estimates in Table 1 were derived by the virtual potential temperature (θ_v) gradient approach, or height of the maximum vertical gradient in θ_v. A mixed layer defined from 10-100 hPa AGL was used in the calculation of LCL, LFC, and PBLh.

We intercompared PBLh estimates from three common approaches: 0.25 critical bulk Richardson number, minimum vertical gradient in relative humidity, and minimum vertical gradient in wind speed. During the nighttime, the PBLh estimates from the wind gradient approach were found to differ substantially from the others, which also had a large spread. Considering that the bulk Richardson number method requires θ_v and horizontal wind components (e.g., Zhang et al. 2014), we decided to try a fourth approach using the maximum vertical gradient in θ_v. Ultimately, this (θ_v gradient) approach yielded the most consistently reasonable PBLh estimates based on our visual analysis of θ_v-, relative humidity-, and wind profiles. Although discrepancies between the automated θ_v gradient approach and visual analysis do occur, they are mostly confined to early morning (i.e., 0530 and 0830 UTC) radiosondes. The lowest 4000 m potential temperature (θ) profiles for all ESLCS radiosondes on a given IOP day are plotted in Appendix A.

Figure 3 illustrates, for the same radiosonde data, the PBLh estimates from this study's θ_v approach (black line) relative to the four PBLh estimates provided by the ARM Planetary Boundary Layer Height Value-Added Product (PBLh VAP) (Sivaraman et al. 2013), which are derived according to: 0.25 critical Richardson number (Seibert et al. 2000), 0.5 critical Richardson number (Seibert et al. 2000), Liu and Liang (2010), and Heffter (1980) methodologies. The PBLh range of the five estimates—for the same radiosonde—was found to span from approximately 100 m to approximately 3000 m (Fig. 3). Clearly, further analysis is required to drill-down into the source of these differences so that the PBLh estimation procedure may be refined and potentially unified (LeMone et al. 2013). The PBLh is a critical input to the land-atmosphere mixing diagram analysis (Betts 1992, Santanello et al. 2009, Stommel 1947): uncertainty in the PBLh translates directly into uncertainty in PBL budgets of heat and moisture as well as entrainment ratios (Santanello et al. 2009).

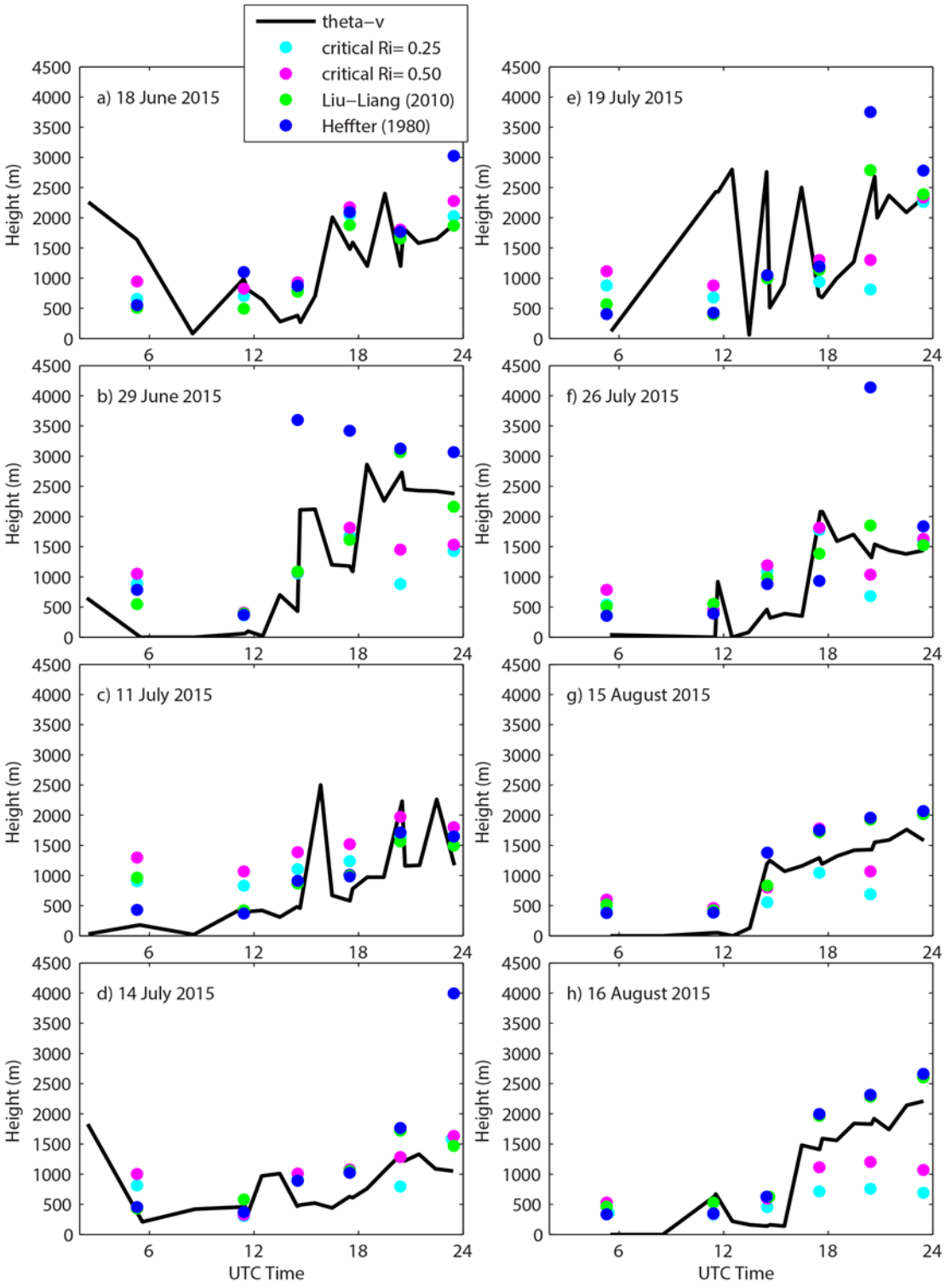

Figure 3. (a-l) PBLh estimates from this study for all radiosondes (black line) and from the ARM PBLh VAP (filled circles) at 0530, 1130, 1730, 2030, and 2330 UTC.

Figure 3 (a-l) (continued)

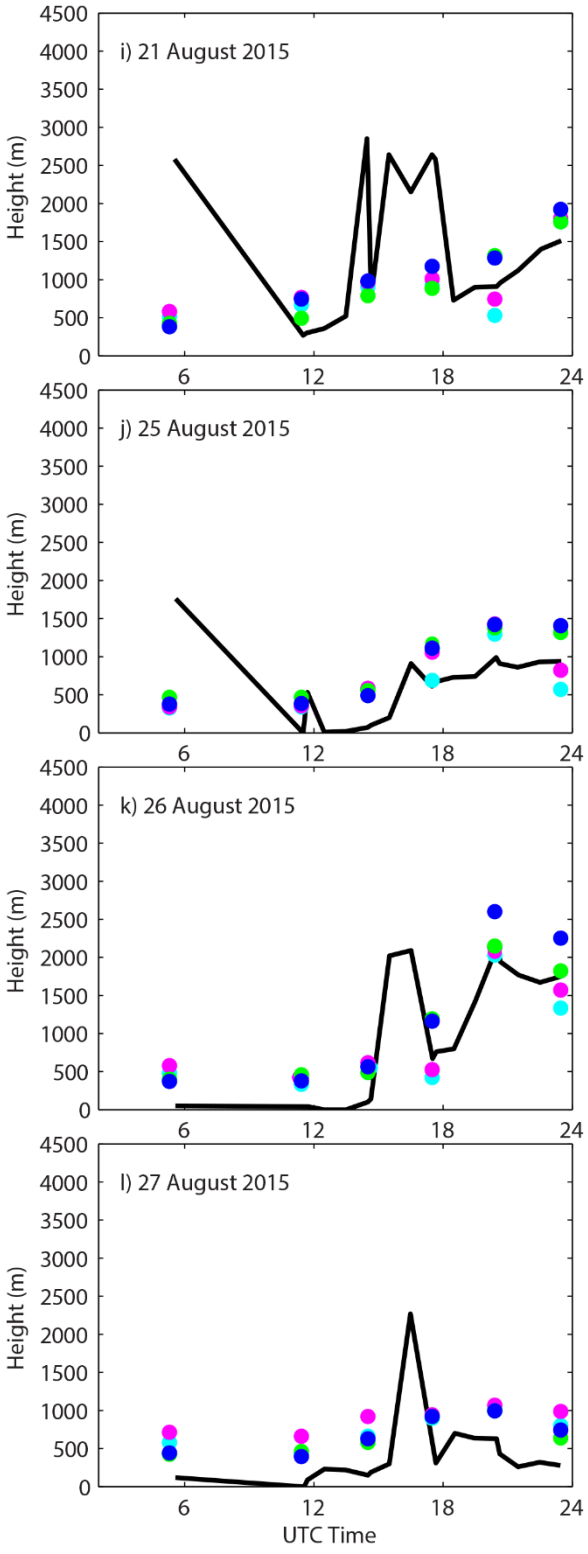

Figure 4(a) illustrates the CTP-HI space sampled during the ESLCS campaign. Recall that IOP days were classified using the NARR CTP-HI over the SGP domain, whereas the ESLCS radiosonde derived CTP-HI is plotted in Fig. 4(a). Figures 4(b) and 4(c) illustrate the difference between 0830 UTC and 1130 UTC radiosonde HI and CTP, respectively. The mean absolute difference (MAD) is 3.3 K for HI and 74 J kg^{-1} for CTP. The 0830-1130 UTC HI differences were less than 1 K, with the exception of Aug 15 (13.5 K) and August 16 (4.0 K). The caveat with these comparisons, of course, is that the sample size (n=6; see Section 3) is extremely limited.

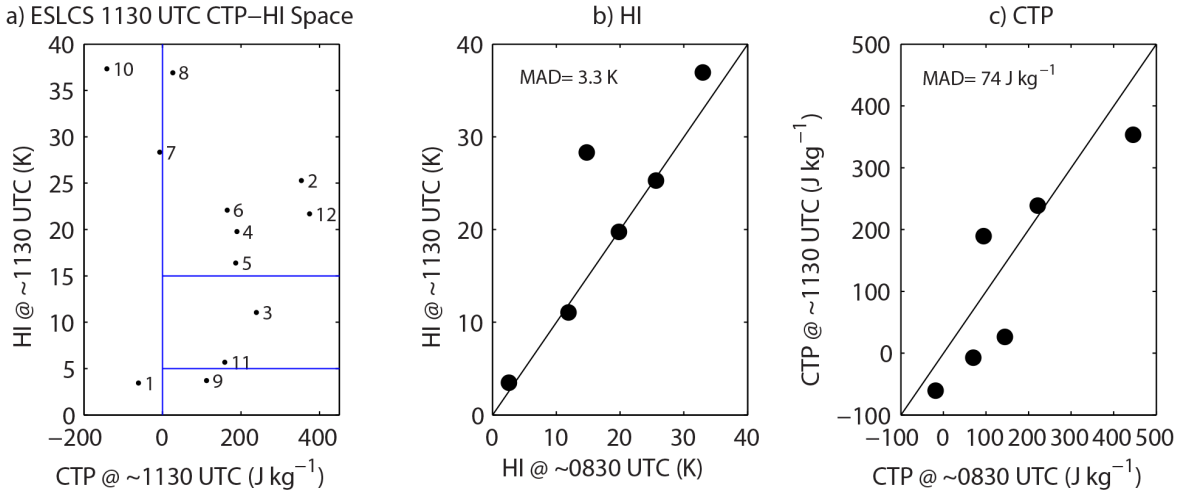

Figure 4. (a) CTP-HI space sampled during the ESLCS campaign. The numbers correspond to the IOP day in chronological order (i.e., 1=18 June, 2= 29 June, etc.). The 5-15 K range in HI is the Findell and Eltahir (2003) suggested range for land surface influence on convective triggering. (b) Intercomparison of 0830 UTC and 1130 UTC HI estimates. (c) Intercomparison of 0830 UTC and 1130 UTC CTP estimates. The mean absolute difference (MAD) for each 6-sample intercomparison is noted in the upper left of panels (b) and (c). 0830 UTC corresponds with the approximate NASA Aqua descending overpass. AIRS is onboard Aqua and was used in Ferguson and Wood (2011) to retrieve estimates of HI and CTP. During the ESLCS campaign, sunrise at ARM-SGP ranged from 1111 UTC (18 June) to 1156 UTC (27 August).

Figure 5 illustrates the diurnal variability of HI (Fig. 5a) and CTP (Fig. 5b) in the form of the anomaly from same-day 1130 UTC values. The 12-day MAD (mean difference) is illustrated with green (blue) circles for 0530, 1430, 1730, 2030, and 2330 UTC. The range of the MAD (mean difference) for HI is 3.7 - 7.2 (-1.3 - 1.0) K. The range of the MAD for CTP is 94 - 195 (8 - 160) J kg^{-1}. During daytime, mean differences in HI tended to decrease and stabilize whereas mean differences in CTP are increasingly positive as the day progresses (Fig. 5).

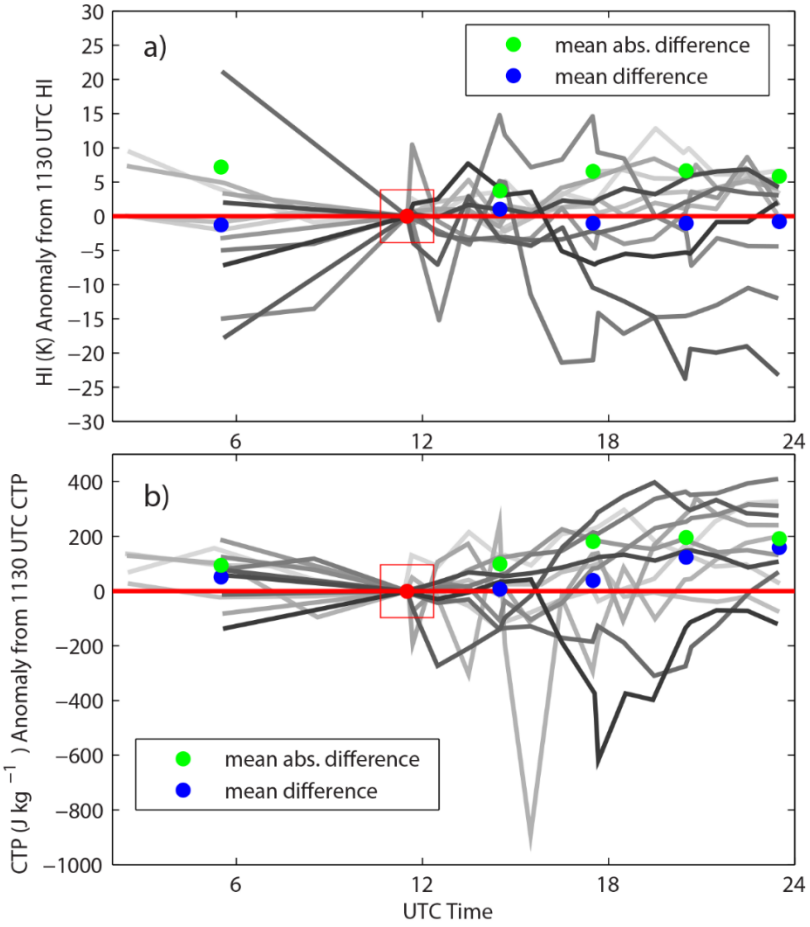

Figure 5. Plot of (a) HI and (b) CTP anomaly from 1130 UTC values for all available ESLCS radiosondes (gray lines). Each shade of gray corresponds to a particular ESLCS IOP day. The MAD (green circles) and mean difference (blue circles) values were computed from the 12 IOP day anomaly values at 0530, 1430, 1730, 2030, and 2330 UTC.

Figure 6 shows the 12-day MAD in temperature (*T*), relative humidity (RH), and specific humidity (*q*) for each of ESLCS's paired launch times (1130/1140, 1430/1440, 1730/1740, and 2030/2040 UTC), as well as the 96-day (12 days x 4 times x 2 radiosondes) aggregate of all paired launches. To prepare the radiosonde profiles for intercomparison, the *T* and RH profiles were first interpolated to a common 10 hPa resolution vertical grid. The interpolated *T* and RH profiles were then used to calculate the corresponding *q* profile. This approach is consistent with the fact that independent sensors on the radiosonde (Vaisala RS41) measure *T* and RH. The maximum (minimum) *q* MAD for the 0-300 hPa layer AGL was observed for the 2030/2040 UTC (1430/1440 UTC) launch times. The *q* MAD magnitude was primarily driven by the inter-radiosonde RH variability. The maximum *T* MAD for the 0-200 hPa layer AGL occurs for 1130/1140 UTC launch pairs and for 200-300 hPa AGL at 1430/1440 UTC, which is consistent with large day-to-day variability in the nocturnal boundary layer at sunrise and in the peak convective boundary layer (CBL) growth at midday. The 96-RAOB aggregate MAD for the lowest 0-100 hPa, 100-200 hPa, and 200-300 hPa AGL are notated on each panel of Fig 6. They are, for *T*, RH, and *q*:

0.24-0.29 K, 2.2-3.4%, and 0.36-0.41 g kg^{-1}, respectively. The MAD of all 10-minute radiosonde pairs is a measure of the SGP warm season 10-minute natural variability, and arguably a candidate accuracy target for ground-based remote profilers, such as the Atmospheric Emitted Radiance Interferometer (AERI) (Turner and Lohnert 2014). Only a few radiosondes did not include levels up to 100 hPa. They were: 11 July 2016 @2040 UTC (416.16 hPa top) and 14 July 2016 @ 1130 UTC (381.66 hPa top).

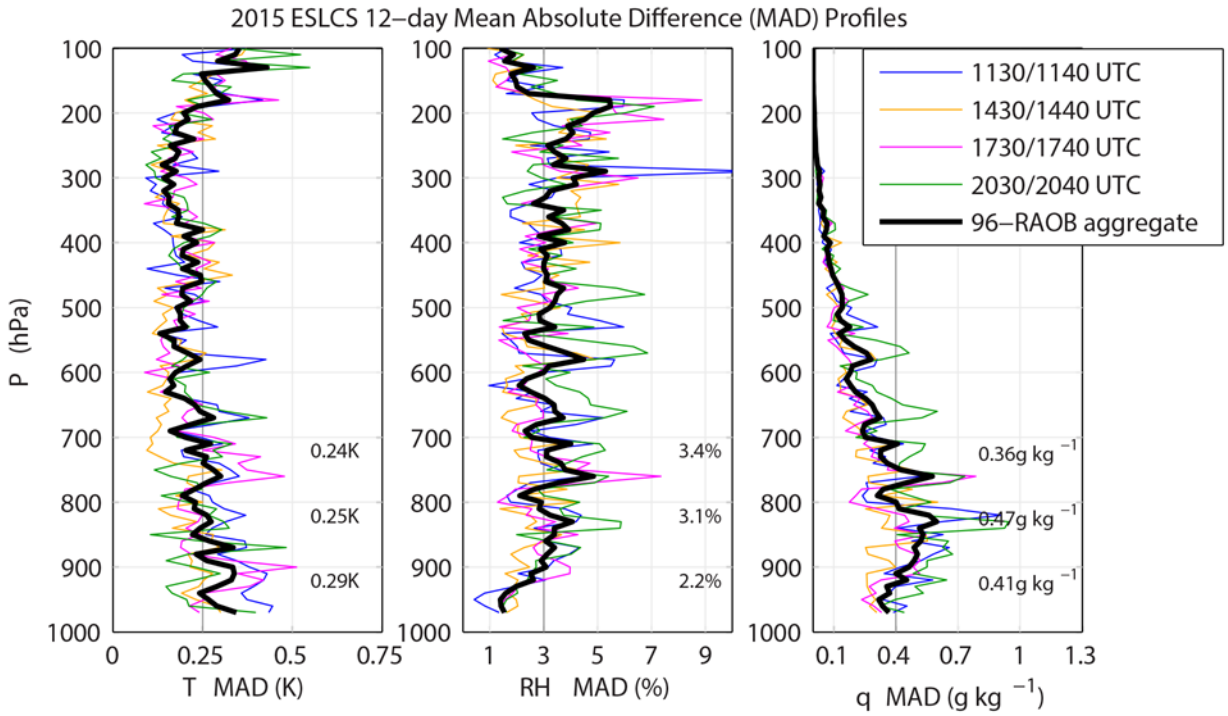

Figure 6. The 12-day T, RH, and q MAD for each of the ESLCS campaign's four paired launch times on a uniform 10 hPa vertical grid.

Appendix B includes, for each IOP day, plots of the *T*, RH, and *q* differences for each pair of 10-minute lagged radiosondes. Large differences between the 10-minute lagged radiosondes typically occur due to one of two reasons. The first reason is that one radiosonde happened to ascend through a structure/layer that was missed by the other radiosonde. For example, the 1730/1740 radiosonde pair on 21 August illustrates such a case with up to 2 K and 30% RH differences in the 700-800 hPa layer. The second and more common reason is sampling in sharp vertical gradients (i.e., PBL top or other inversion layer) occurring in thin 10-15 hPa layers. Such features are resolved by the 12-m vertical resolution (throughout the profile) of the radiosonde. For example, the 1730/1740 15 August radiosondes illustrate a case for which the paired radiosonde disagreement is isolated to a single level (850 hPa) with a 1 K difference in *T*. While the high vertical resolution of the radiosondes enabled thin layers to be resolved, it also challenged our automated LFC and PBLh search algorithms to distinguish large-scale gradients (i.e., in θ_v) from local noise.

5.0 Future Work

Our analysis of the ESLCS data to date has highlighted the need for several additional studies. There is a need to:

1. Better understand PBLh uncertainties and if possible arrive at a community consensus on a best-practice methodology. Intercomparison demands consistency in PBLh estimates across models, radiosondes, and remote-sensing profilers. Relatedly, there is a need to quantify uncertainty associated with fitting a diurnal cycle curve of PBLh to only 1 or 2 radiosonde-based estimates, as is current practice.
2. Revisit the CTP-HI coupling classification framework with due consideration given to the prevailing synoptic and mesoscale conditions.
3. Perform cross-validation of ESLCS radiosonde *T*, RH, and wind profiles and coincident ARM-SGP CF remote sensing profiler estimates (e.g., AERI, Raman lidar, and Doppler lidar) to assess the applicability of these profilers for land-atmosphere studies.
4. Confront numerical weather models with the ESLCS-derived diurnal evolution of thermodynamic profiles.

Such studies should be considered a starting point, rather than a complete list.

6.0 Public Outreach

The ESLCS campaign was highlighted in an *ARM News* article entitled, “Up, up, and Away”, written by Hanna Goss and published on July 6, 2015 (Goss 2015). Screenshots of the full article are provided as Appendix C. The campaign’s science plan and data set may be accessed through the following ARM website: (https://www.arm.gov/campaigns/sgp2015eslcs).

7.0 ESLCS Campaign Presentations

Initial results from the ESLCS campaign were presented at the 2015 Fall Meeting of the American Geophysical Union (Ferguson et al. 2015):

Ferguson, CR, H-J Song, and JK Roundy. 2015. “Understanding land-atmosphere coupling and its predictability at the ARM Southern Great Plains site.” A31I-05, AGU Fall Meeting, December 2015.

8.0 Appendix A

For each ESLCS IOP day, the lowest 4000 m potential temperature (θ) profiles for all IOP day radiosondes are given. The launch times of all plotted radiosondes are listed on the left side of each plot. The nominal 1130, 1430, 1730, and 2030 UTC radiosondes are called out with blue, orange, magenta, and

green lines, respectively. All other radiosondes are represented by a unique shade of gray, which scales linearly from dark gray at 0230 UTC to light gray at 2330 UTC.

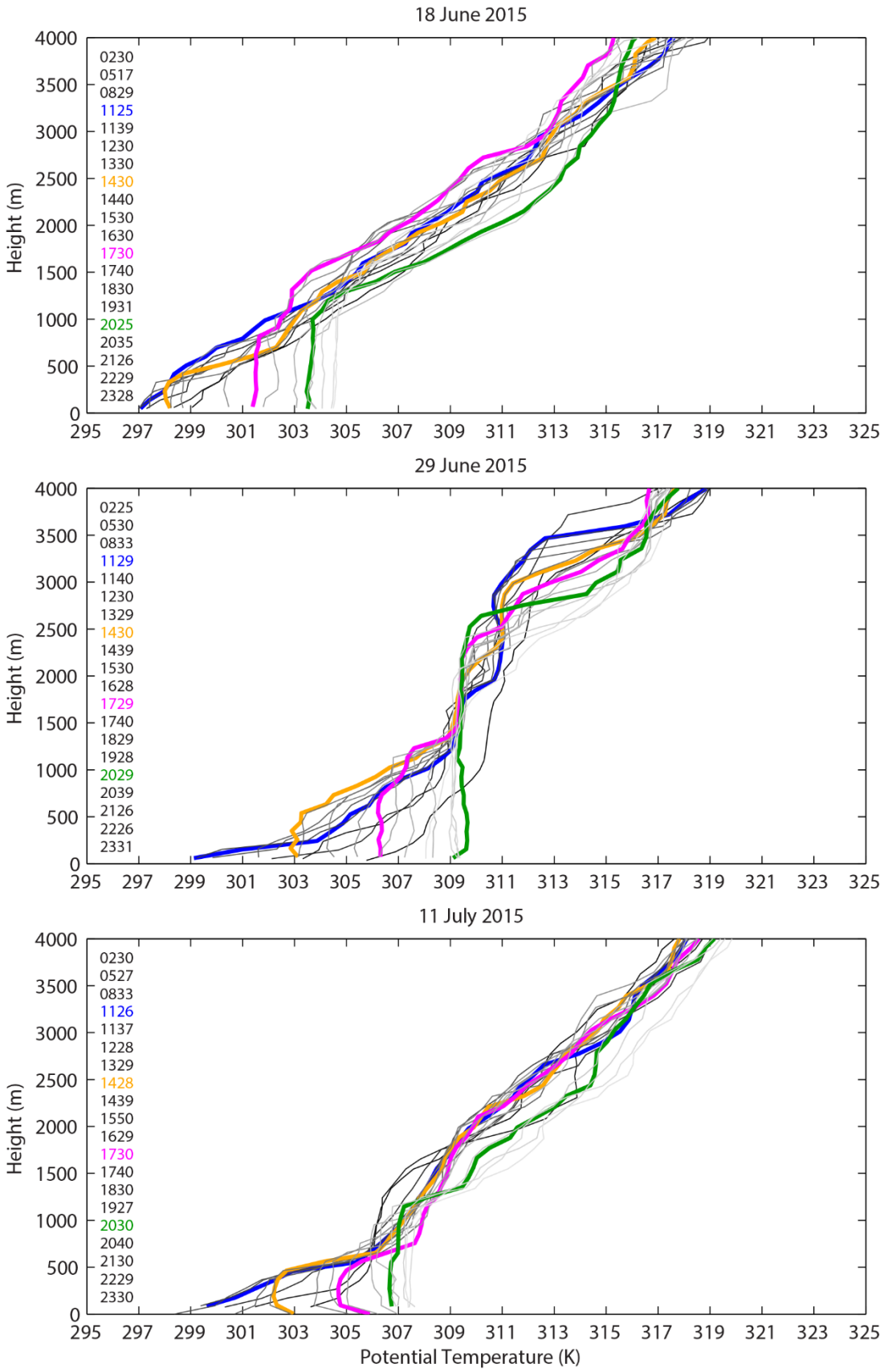
18 June 2015
0230
0517
0829
1125
1139
1230
1330
1430
1440
1530
1630
1730
1740
1830
1931
2025
2035
2126
2229
2328
29 June 2015
0225
0530
0833
1129
1140
1230
1329
1430
1439
1530
1628
1729
1740
1829
1928
2029
2039
2126
2226
2331
11 July 2015
0230
0527
0833
1126
1137
1228
1329
1428
1439
1550
1629
1730
1740
1830
1927
2030
2040
2130
2229
2330
Height (m)
Potential Temperature (K)

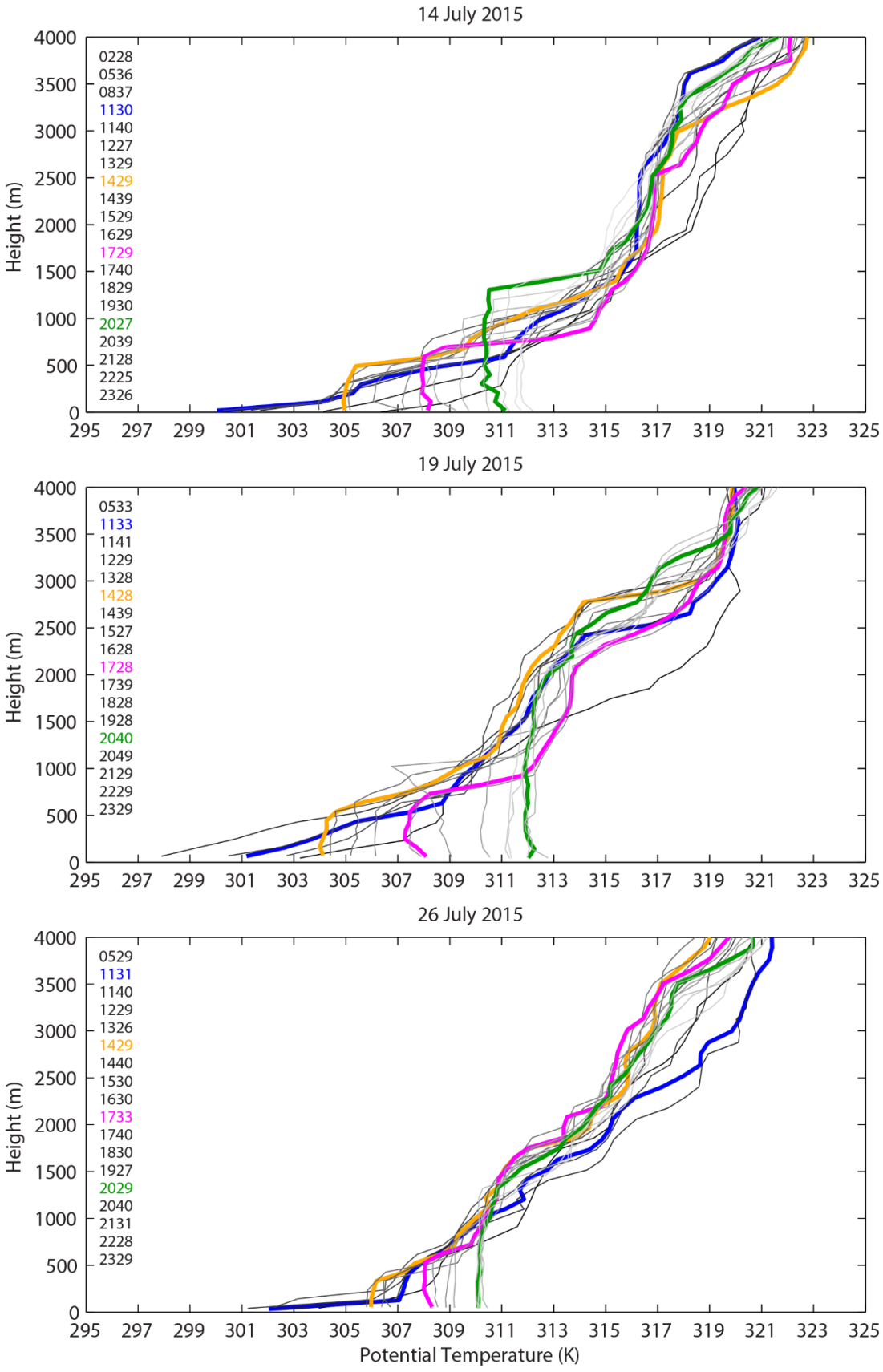
14 July 2015
0228
0536
0837
1130
1140
1227
1329
1429
1439
1529
1629
1729
1740
1829
1930
2027
2039
2128
2225
2326
19 July 2015
0533
1133
1141
1229
1328
1428
1439
1527
1628
1728
1739
1828
1928
2040
2049
2129
2229
2329
26 July 2015
0529
1131
1140
1229
1326
1429
1440
1530
1630
1733
1740
1830
1927
2029
2040
2131
2228
2329
Height (m)
Potential Temperature (K)

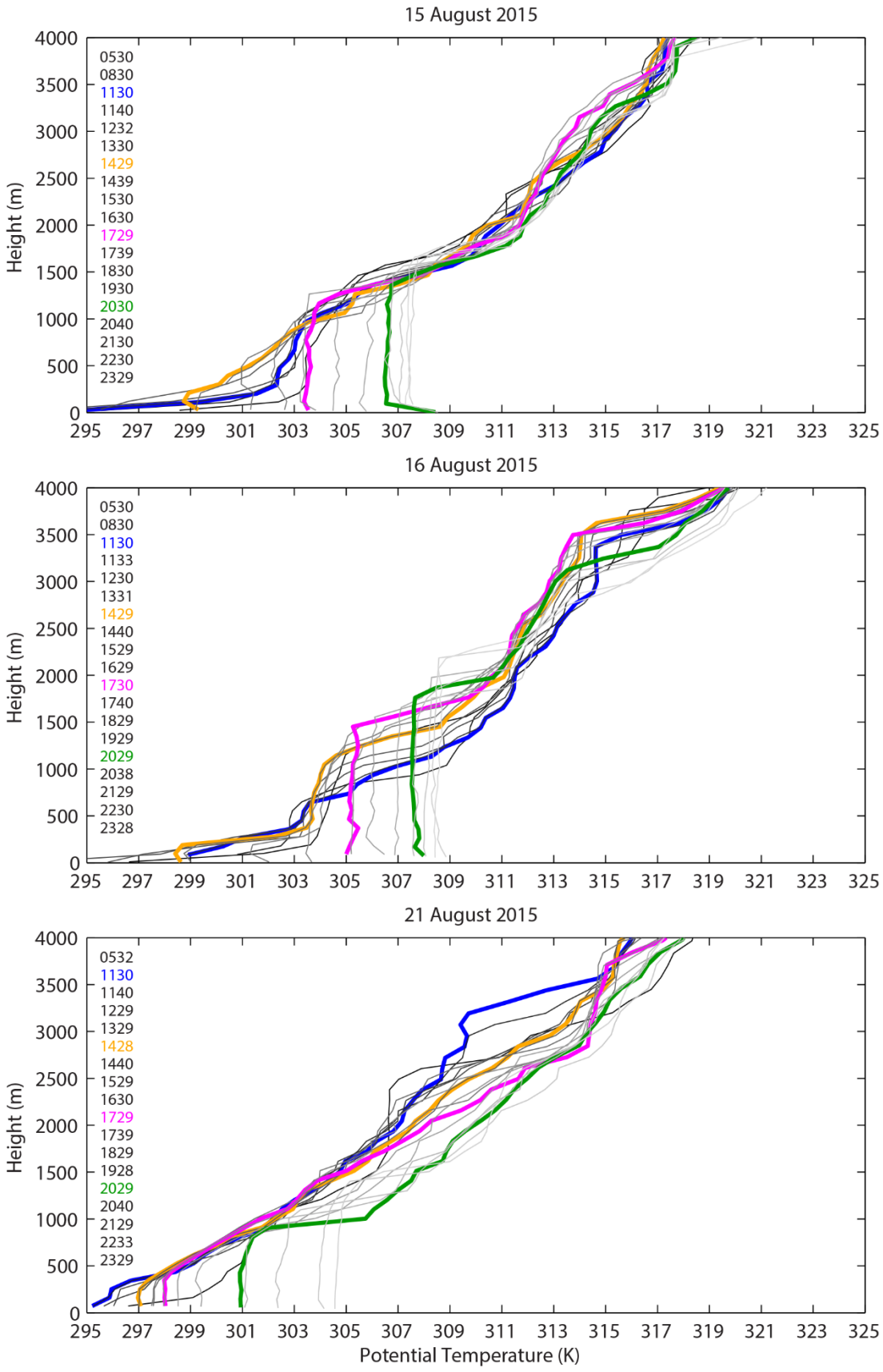
15 August 2015
0530
0830
1130
1140
1232
1330
1429
1439
1530
1630
1729
1739
1830
1930
2030
2040
2130
2230
2329
16 August 2015
0530
0830
1130
1133
1230
1331
1429
1440
1529
1629
1730
1740
1829
1929
2029
2038
2129
2230
2328
21 August 2015
0532
1130
1140
1229
1329
1428
1440
1529
1630
1729
1739
1829
1928
2029
2040
2129
2233
2329
Height (m)
Potential Temperature (K)

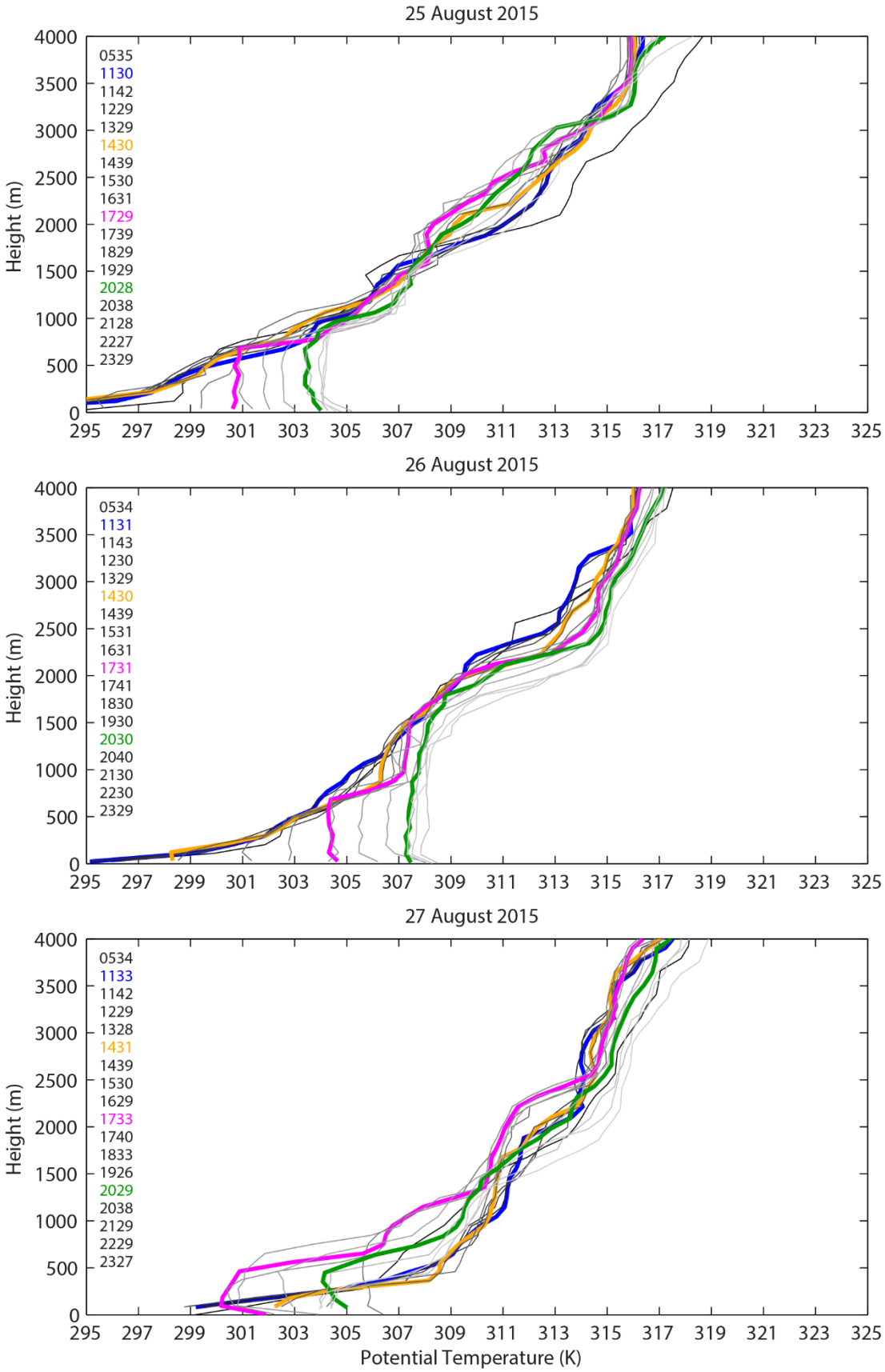
25 August 2015
0535
1130
1142
1229
1329
1430
1439
1530
1631
1729
1739
1829
1929
2028
2038
2128
2227
2329
26 August 2015
0534
1131
1143
1230
1329
1430
1439
1531
1631
1731
1741
1830
1930
2030
2040
2130
2230
2329
27 August 2015
0534
1133
1142
1229
1328
1431
1439
1530
1629
1733
1740
1833
1926
2029
2038
2129
2229
2327
Height (m)
Potential Temperature (K)

9.0 Appendix B

For each ESLCS IOP day, the mean absolute difference (MAD) between 10-minute lagged radiosonde pairs at 1130/1140 (blue), 1430/1440 (orange), 1730/1740 (magenta), and 2030/2040 UTC (green), as well as the mean of these 4 values (black), is given. As for Fig. 6, the radiosonde *T* and RH profiles are first interpolated to a common 10 hPa vertical grid and then a corresponding *q* profile is calculated.

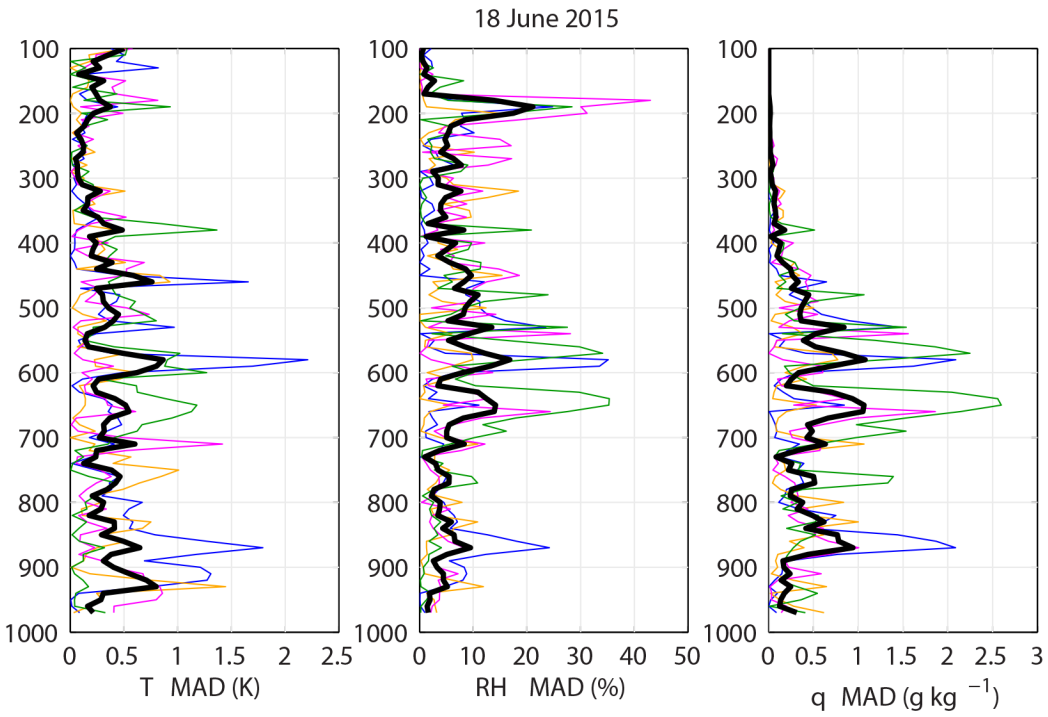
18 June 2015
100
200
300
400
500
600
700
800
900
1000
0 0.5 1 1.5 2 2.5
T MAD (K)
0 10 20 30 40 50
RH MAD (%)
0 0.5 1 1.5 2 2.5 3
q MAD (g kg −1)

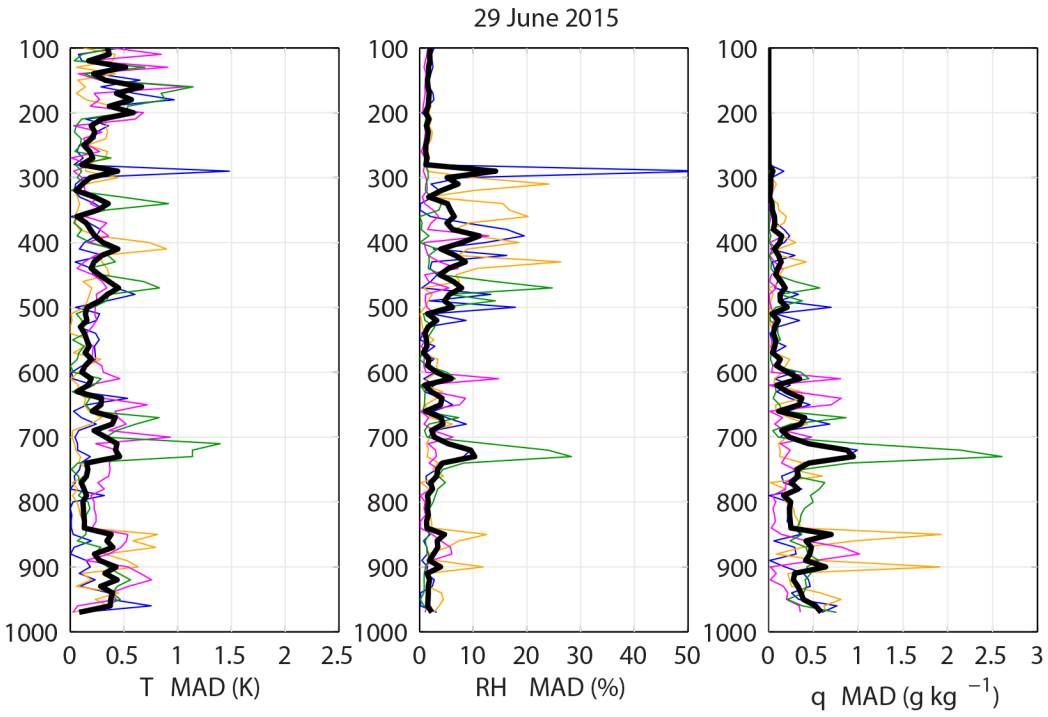
29 June 2015
100
200
300
400
500
600
700
800
900
1000
0 0.5 1 1.5 2 2.5
T MAD (K)
0 10 20 30 40 50
RH MAD (%)
0 0.5 1 1.5 2 2.5 3
q MAD (g kg −1)

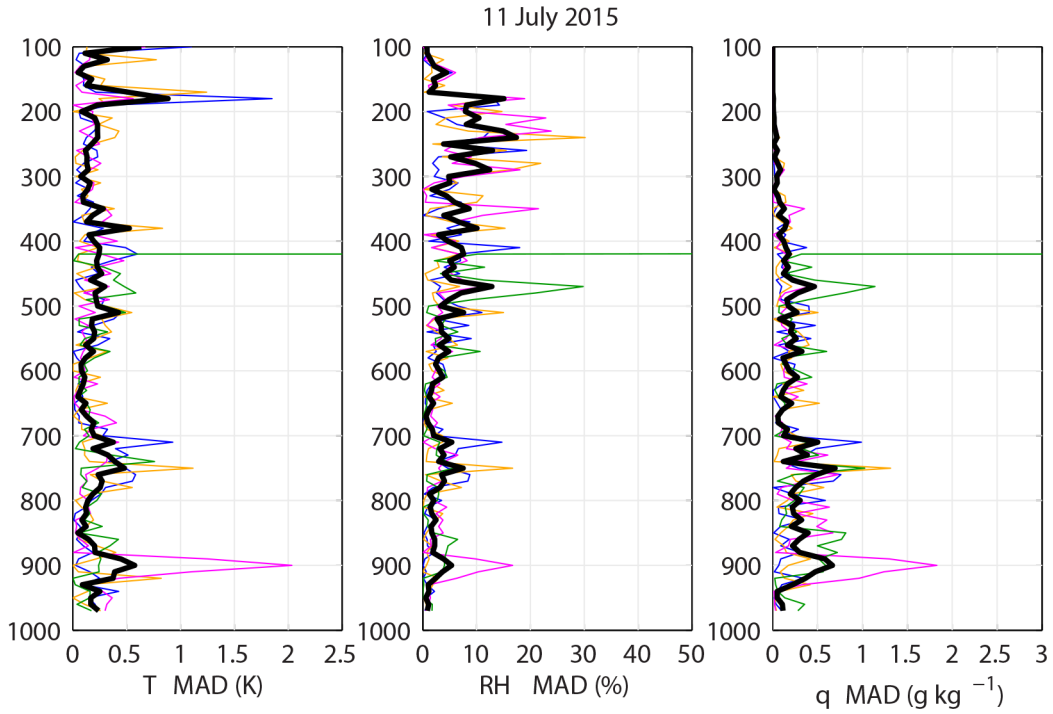
11 July 2015
100
200
300
400
500
600
700
800
900
1000
0 0.5 1 1.5 2 2.5
T MAD (K)
0 10 20 30 40 50
RH MAD (%)
0 0.5 1 1.5 2 2.5 3
q MAD (g kg −1)

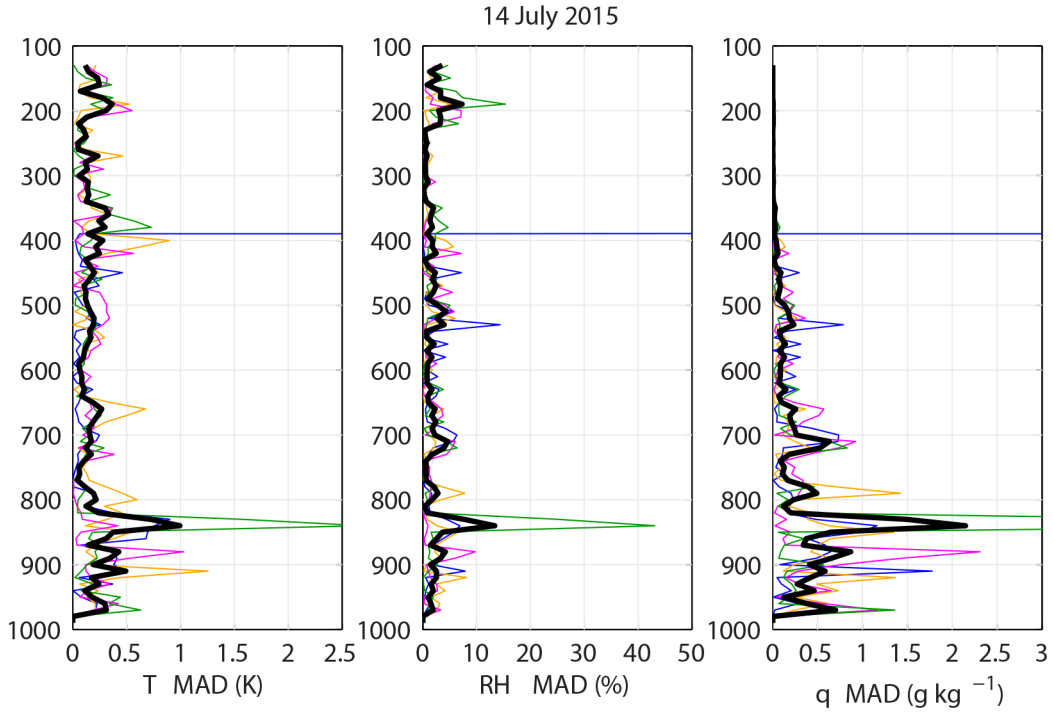
14 July 2015
100
200
300
400
500
600
700
800
900
1000
0 0.5 1 1.5 2 2.5
T MAD (K)
0 10 20 30 40 50
RH MAD (%)
0 0.5 1 1.5 2 2.5 3
q MAD (g kg −1)

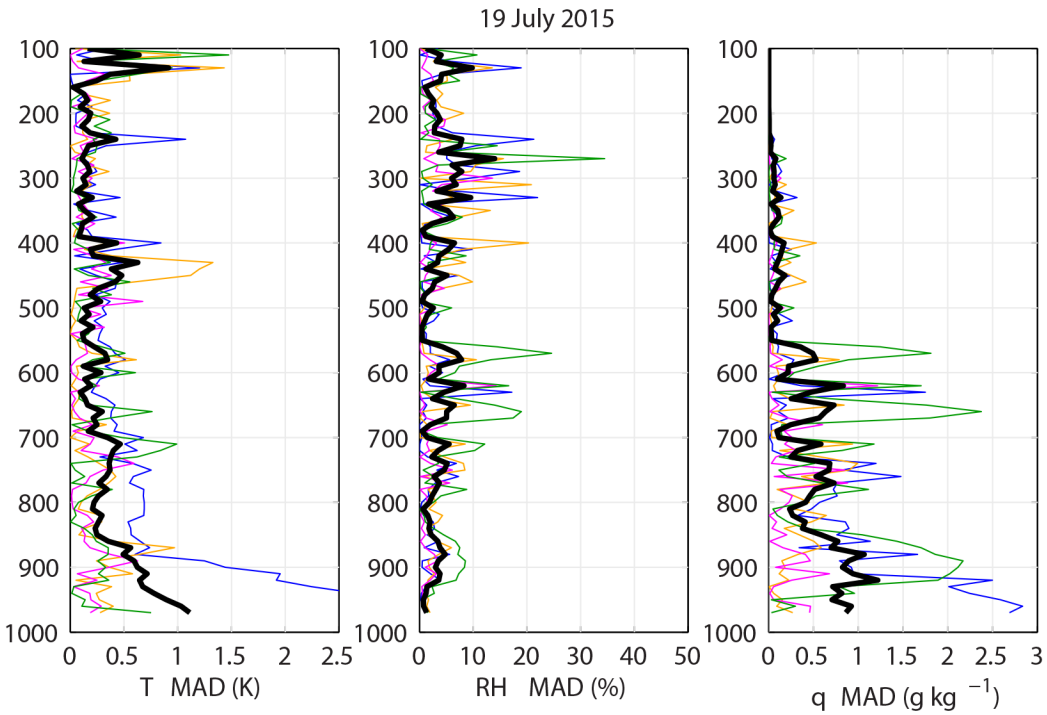
19 July 2015
100
200
300
400
500
600
700
800
900
1000
0 0.5 1 1.5 2 2.5
T MAD (K)
0 10 20 30 40 50
RH MAD (%)
0 0.5 1 1.5 2 2.5 3
q MAD (g kg −1)

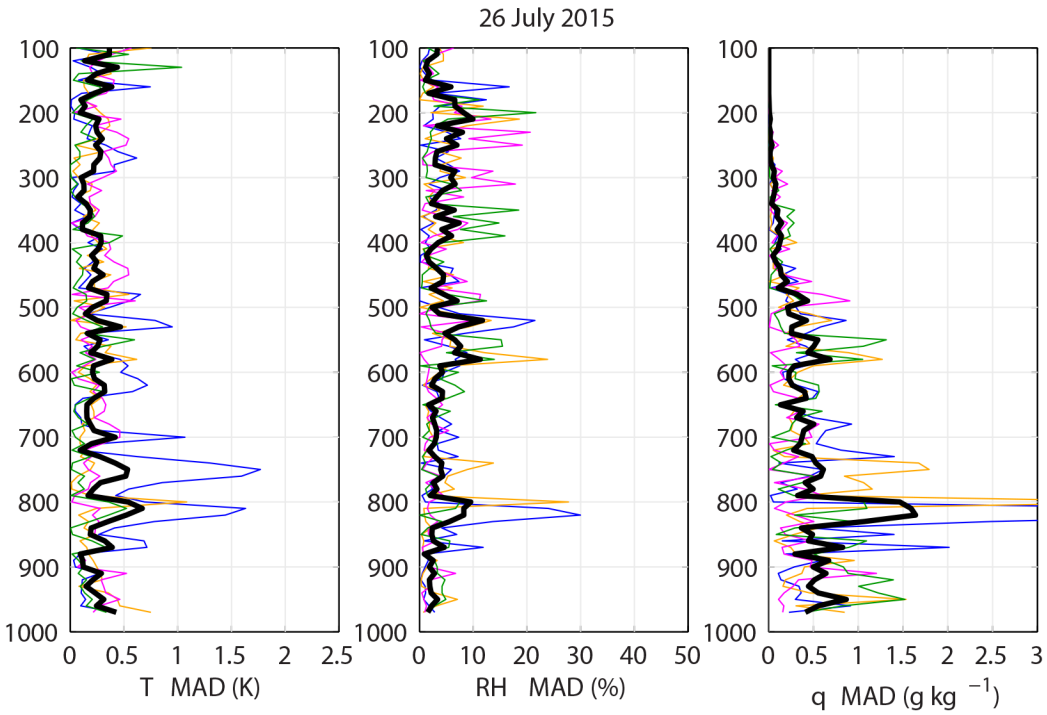
26 July 2015
100
200
300
400
500
600
700
800
900
1000
0 0.5 1 1.5 2 2.5
T MAD (K)
0 10 20 30 40 50
RH MAD (%)
0 0.5 1 1.5 2 2.5 3
q MAD (g kg −1)

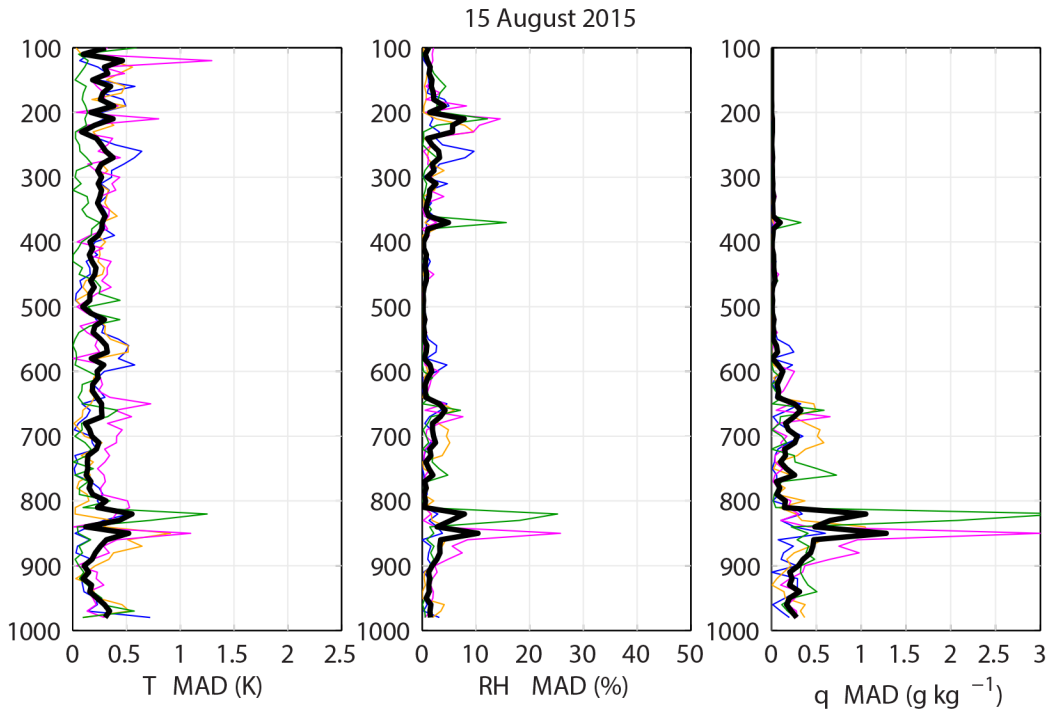
15 August 2015
100
200
300
400
500
600
700
800
900
1000
0 0.5 1 1.5 2 2.5
T MAD (K)
0 10 20 30 40 50
RH MAD (%)
0 0.5 1 1.5 2 2.5 3
q MAD (g kg −1)

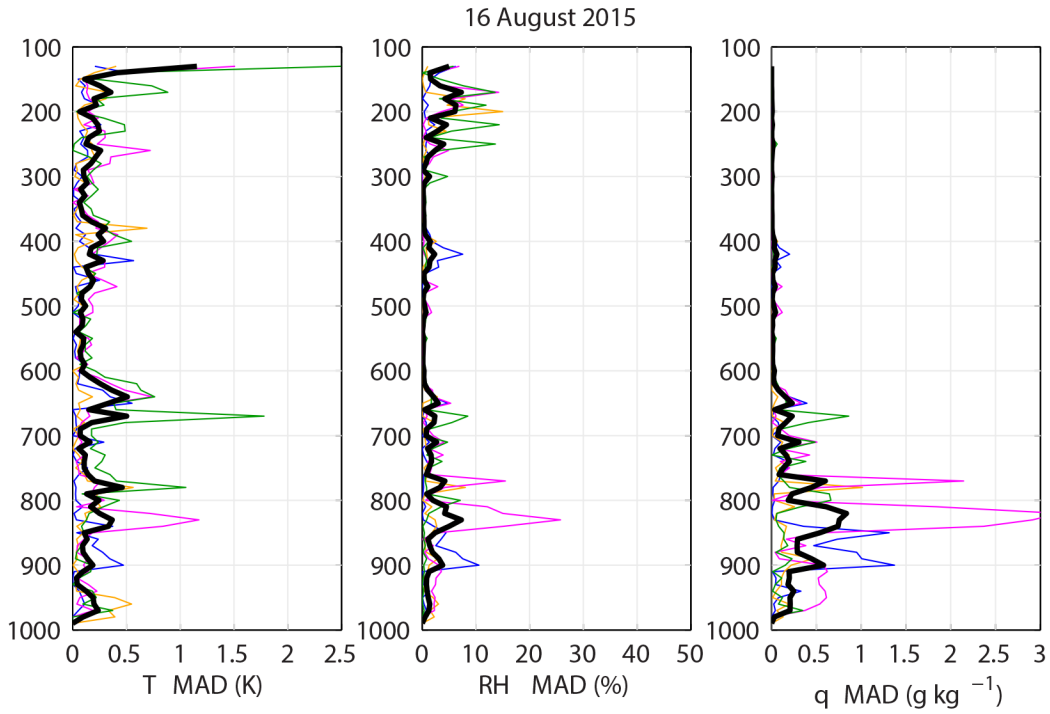
16 August 2015
100
200
300
400
500
600
700
800
900
1000
0 0.5 1 1.5 2 2.5
T MAD (K)
0 10 20 30 40 50
RH MAD (%)
0 0.5 1 1.5 2 2.5 3
q MAD (g kg −1)

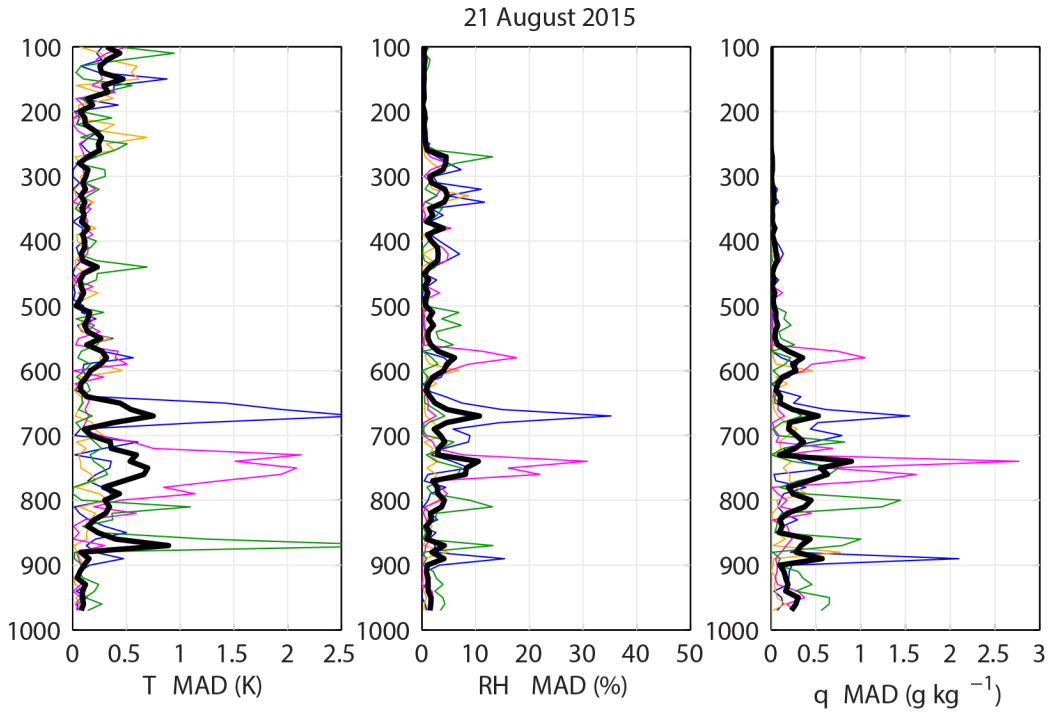
21 August 2015
100
200
300
400
500
600
700
800
900
1000
0 0.5 1 1.5 2 2.5
T MAD (K)
0 10 20 30 40 50
RH MAD (%)
0 0.5 1 1.5 2 2.5 3
q MAD (g kg −1)

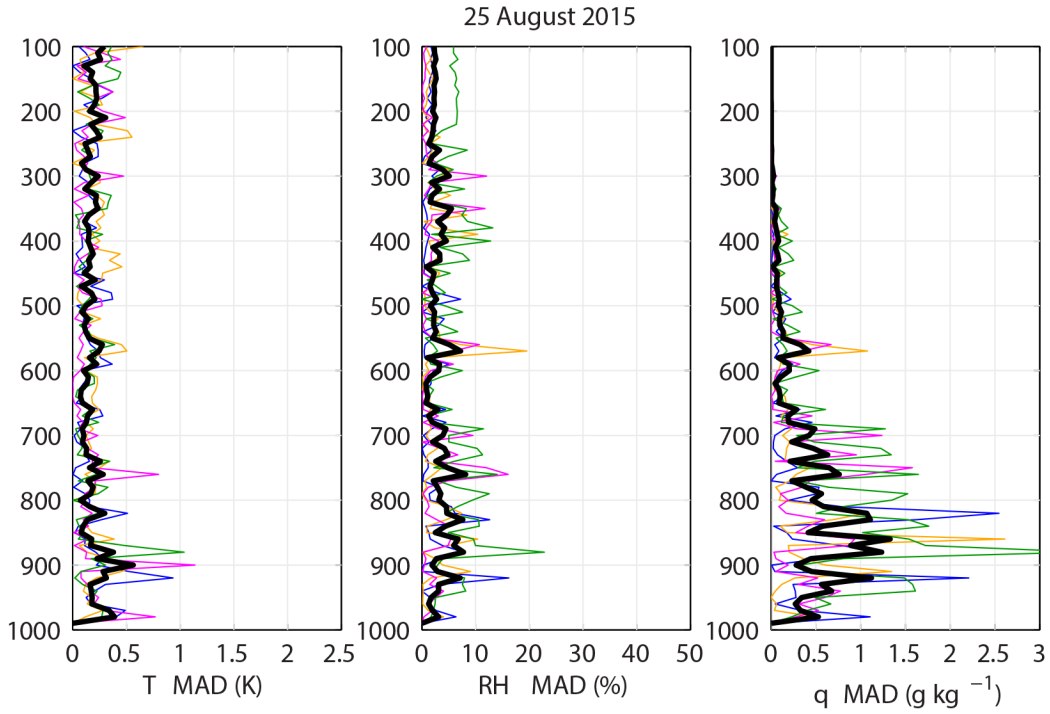
25 August 2015
100
200
300
400
500
600
700
800
900
1000
0 0.5 1 1.5 2 2.5
T MAD (K)
0 10 20 30 40 50
RH MAD (%)
0 0.5 1 1.5 2 2.5 3
q MAD (g kg −1)

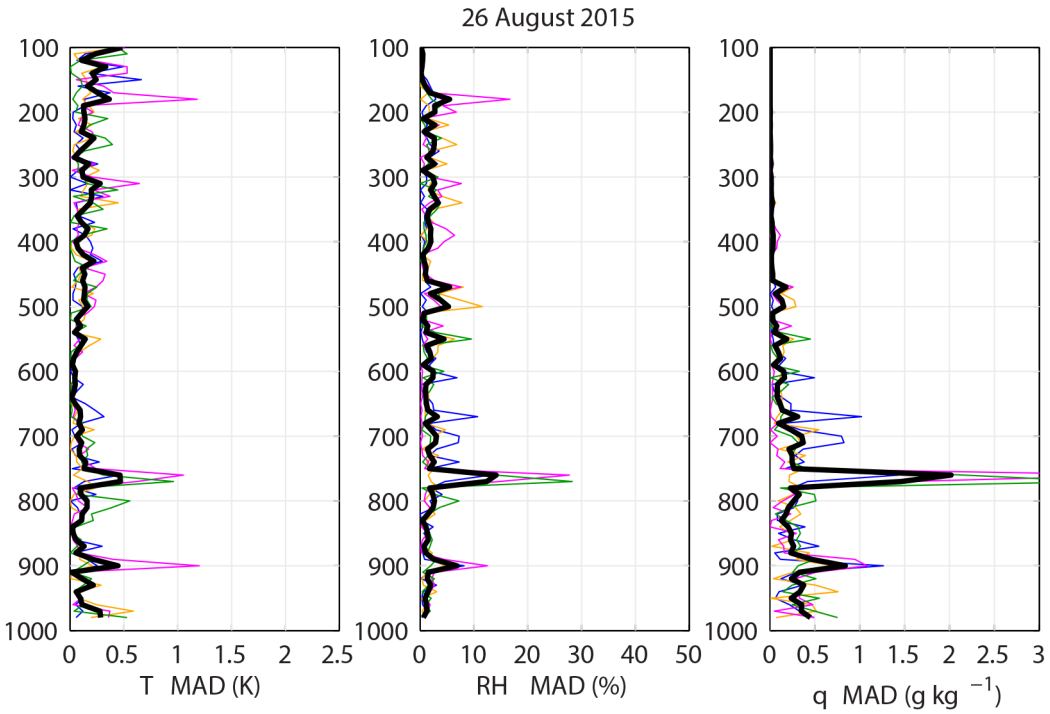
26 August 2015
100
200
300
400
500
600
700
800
900
1000
0 0.5 1 1.5 2 2.5
T MAD (K)
0 10 20 30 40 50
RH MAD (%)
0 0.5 1 1.5 2 2.5 3
q MAD (g kg −1)

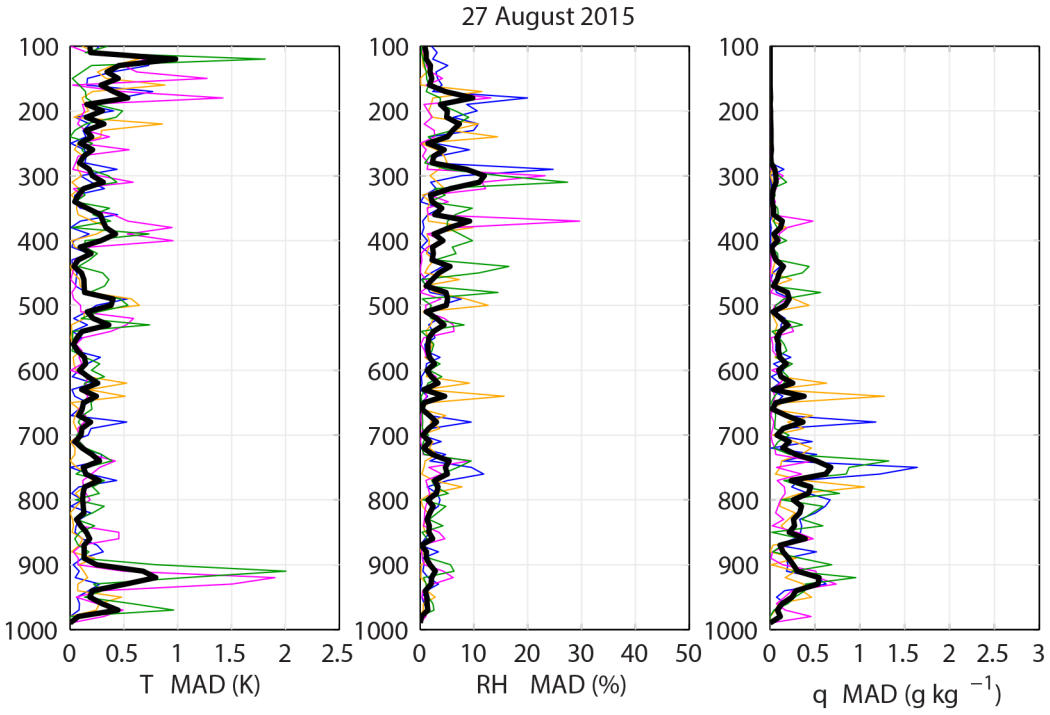
27 August 2015
100
200
300
400
500
600
700
800
900
1000
0 0.5 1 1.5 2 2.5
T MAD (K)
0 10 20 30 40 50
RH MAD (%)
0 0.5 1 1.5 2 2.5 3
q MAD (g kg −1)

10.0 Appendix C

The *ARM News* article entitled, "Up, up, and Away", written by Hanna Goss and published on July 6, 2015 (Goss 2015).

July 6, 2015 [Feature Stories and Releases]

Up, Up, and Away!

SHARE

Using weather balloons to improve understanding of how surface conditions may impact clouds and rain

This summer, researchers are launching an unprecedented number of weather balloons in rural Oklahoma to collect data to help improve how weather and climate models predict the diurnal cycle of rainfall and cloud development.

Weather balloons, also called sondes, will be launched hourly from 6:30 am to 6:30 pm for 12 selected days between June 15 and August 31, 2015, to gather data to improve how weather and climate models predict the diurnal cycle of rainfall and cloud development.

A diurnal cycle is any pattern that recurs every 24 hours as a result of one full rotation of the Earth with respect to the sun. In climatology, the diurnal cycle is one of the most basic forms of climate patterns, yet can be a challenge for weather and climate models to get right. The diurnal cycles of surface temperature, humidity, and rainfall are the result of complex interactions between the land surface and the lowest levels of the atmosphere.

"The diurnal cycle of rainfall and cloud development has a sizable impact on our ability to predict climate and the duration and severity of extremes, such as floods and drought," said Craig Ferguson, a research assistant professor at the University at Albany's Atmospheric Sciences Research Center in New York and the lead investigator for the field research campaign Enhanced Soundings for Local Coupling Studies.

Rural Oklahoma is home to the ARM Facility's Southern Great Plains site, which will host the Enhanced Soundings field campaign this summer.

Climate models are challenged with accurately predicting the timing and amplitude of the cycle because rain during the day versus night has different interactions with the land. For example, precipitation that is too frequent, too light, and peaks during daytime leads to increased infiltration and reduced runoff, enhanced evapotranspiration, and accelerates soil moisture dry-down.

"Over time," Ferguson explained, "this plays a big role on the ability of a climate model to predict the persistence of drought and rain events."

"To challenge the models," he said, "we want a data set spanning multiple days that provides high temporal and vertical resolution of the atmosphere from the early morning hours to the end of day, and we are targeting days with synoptic [view at a common point] conditions that are conducive to local land affects."

Gold Standard for Profiling

To get these data, Ferguson and co-investigators, Pierre Gentine from Columbia University in New York and Joseph Santanello from NASA's Goddard Space Flight Center in Maryland, will select 12 campaign days between June 15 and August 31 to augment operational radiosonde launches at the Southern Great Plains (SGP), the premier field measurement site of the Atmospheric Radiation Measurement (ARM) Climate Research Facility.

"The radiosonde is still the gold standard for profiling from the land's surface to the highest levels of atmosphere," Ferguson said.

Radiosondes, like this one, are attached to weather balloons to collect vertical profiles (data sets) of both the thermodynamic state of the atmosphere and wind speed and direction.

Due to their expense, radiosondes are typically only launched every 6 hours at the ARM SGP site and every 12 hours at the 102 National Weather Service sites nationally. To get a more robust data set, the Enhanced Soundings researchers will launch radiosondes hourly from 6:30 am to 6:30 pm. At 3-hour intervals a duplicate "trailer" radiosonde will be launched 10 minutes later to make sure a representative profile of the atmosphere is being captured. A single launch at 3:30 am will correspond with the nighttime overpass of the NASA Afternoon Earth-observing satellite constellation (A-Train) that includes the Atmospheric Infrared Sounder (AIRS), which estimates atmospheric profiles of temperature and humidity by remote sensing.

In total, 19 balloons will be launched on each research day, including the 4 that are launched daily at the ARM site. The selected days that the balloons will be launched are determined by the investigators by 7 am on the preceding day, taking into consideration daily weather forecasts and the operability of complimentary ARM instrumentation.

Big Research Impact

An overarching goal of the Enhanced Soundings campaign is to address how ARM could better observe land-atmosphere interactions and coupling to support the evaluation and refinement of coupled weather and climate models.

The study is running at the SGP concurrently with—and its results will be complimentary to—the Plains Elevated Convection at Night (PECAN), a multi-agency research campaign using airborne, and fixed and mobile ground instrumentation to take detailed measurements of what triggers clouds and precipitation at night.

There is evidence that the initial development of the nocturnal boundary layer strongly depends on the characteristics of the daytime boundary layer, and both the Enhanced Coupling campaign and 24/7 operations of the Atmospheric Emitted Radiance Interferometers (AERIs) during PECAN will provide data to investigate this hypothesis. These two data sets will provide scientists with a rich description of the full diurnal cycle of the atmosphere to study for many years to come.

11.0 References

Betts, AK, 1992. "FIFE atmospheric boundary layer budget methods." *Journal of Geophysical Research-Atmospheres* 97(D17): 523-531, doi:10.1029/91JD03172.

DOE-BER, 2012. Biological and Environmental Research Climate and Environmental Sciences Division Strategic Plan, DOE/SC-0151, http://science.energy.gov/~/media/ber/pdf/CESD-StratPlan-2012.pdf. U.S. Department of Energy Office of Science.

Ek, MB, KE Mitchell, Y Lin, E Rogers, P Grunmann, V Koren, G Gayno and JD Tarpley. 2003. "Implementation of Noah land surface model advances in the National Centers for Environmental

Prediction operational mesoscale Eta model." *Journal of Geophysical Research-Atmospheres*, 108: D22, doi:10.1029/2002.JD003296.

Ferguson, CR, and EF Wood. 2011. "Observed land-atmosphere coupling from satellite remote sensing and reanalysis." *Journal of Hydrometeorol*ogy 12:1221-1254, doi:10.1175/2011JHM1380.1.

Ferguson, CR, J Santanello, and P Gentine. GEWEX-GLASS Local Coupling (LoCo) Southern Great Plains (SGP) Diagnostics Testbed Data Survey, https://docs.google.com/forms/d/1vK31mCCJXU15A2_OdXRmGmp3CcWouH_ooYZft0HYshk/viewform

Ferguson, CR, J Santanello, and P Gentine. 2014. "Enhanced Soundings for Local Coupling Studies: 2015 ARM Climate Research Facility Field Campaign." DOE/SC-ARM-15-035. 8pgs. https://www.arm.gov/publications/programdocs/doe-sc-arm-15-035.pdf

Ferguson, CR, H-J Song, and JK Roundy. 2015. "Understanding land-atmosphere coupling and its predictability at the ARM southern Great Plains site." A31I-05, American Geophysical Union Fall Meeting, December 2015.

Findell, KL, and EAB Eltahir. 2003a. "Atmospheric controls on soil moisture-boundary layer interactions. Part I: Framework development." *Journal of Hydrometeorol*ogy 4: 552-569, doi:10.1175/1525-7541(2003)004<0552:ACOSML>2.0.CO;2.

Findell, KL, and EAB Eltahir. 2003b. "Atmospheric controls on soil moisture-boundary layer interactions. Part II: Feedbacks within the continental United States." *Journal of Hydrometeorol*ogy 4: 570-583, doi:10.1175/1525-7541(2003)004<0570:ACOSML>2.0.CO;2.

Frye, JD, and TL Mote. 2010. "Convection initiation along soil moisture boundaries in the Southern Great Plains." *Monthly Weather Review* 138: 1140-1151, doi:10.1175/2009MWR2865.1.

Geerts, B, DB Parsons, C Ziegler, D Turner, and R Ferrare. 2013. "Plains elevated convection at night (PECAN): Experimental design overview." 37 pages. https://www.eol.ucar.edu/projects/pecan/documents/PECAN_EDO_2013.pdf

Goss, H. 2015. "Up, up, and away! Using weather balloons to improve understanding of how surface conditions may impact clouds and rain," ARM Climate Research Facility https://www.arm.gov/news/features/post/34154

Guo, ZC, PA Dirmeyer, RD Koster, YC Sud, G Bonan, KW Oleson, E Chan, D Verseghy, P Cox, CT Gordon, JL McGregor, S Kanae, E Kowalczyk, D Lawrence, P Liu, D Mocko, C-H Lu, K Mitchell, S Malyshev, B McAvaney, T Oki, T Yamada, A Pitman, CM Taylor, R Vasic, and Y Xue. 2006. "GLACE: The Global Land-Atmosphere Coupling Experiment. Part II: Analysis." *Journal of Hydrometeorology* 7: 611-625, doi:10.1175/JHM511.1.

Heffter, JL. 1980. "Transport layer depth calculations." Second Joint Conference on Applications of Air Pollution Meteorology, New Orleans, LA, USA.

Hendrickx, J, and J Kleissl. 2015. "DOE-ARM Campaign: Scintillometry and soil moisture remote sensing." https://www.arm.gov/campaigns/sgp2015ssmrs.

Koster, RD, PA Dirmeyer, Z Guo, G Bonan, E Chan, P Cox, CT Gordon, S Kanae, E Kowalczyk, D Lawrence, P Liu, C-H Lu, S Malyshev, B McAvaney, K Mitchell, D Mocko, T Oki, K Oleson, A Pitman, YC Sud, CM Taylor, D Verseghy, R Vasic, Y Xue, and T Yamada. 2004. "Regions of strong coupling between soil moisture and precipitation." *Science*, 305(5687), 1138-1140, doi:10.1126/science.1100217.

Koster, RD, YC Sud, Z Guo, PA Dirmeyer, G Bonan, KW Oleson, E Chan, D Verseghy, P Cox, H Davies, E Kowalczyk, CT Gordon, S Kanae, D Lawrence, P Liu, D Mocko, C-H Lu, K Mitchell, S Malyshev, B McAvaney, T Oki, T Yamada, A Pitman, CM Taylor, R Vasic, and Y Xue. 2006. "GLACE: The Global Land-Atmosphere Coupling Experiment. Part I: Overview." *Journal of Hydrometeorology* 7, 590-610, doi:10.1175/JHM510.1.

LeMone, MA, M Tewari, F Chen, and J Dudhia. 2013. "Objectively determined fair-weather CBL depths in the ARW-WRF model and their comparison to CASES-97 observations." *Monthly Weather Review*, 141**:** 30-54, doi:10.1175/MWR-D-12-00106.1.

Liu, SY, and XZ Liang. 2010. "Observed diurnal cycle climatology of planetary boundary layer height." *Journal of Climate*, 23: 5790-5809, doi:10.1175/2010JCLI3552.1.

McManus, GD, MA Shafer, and M Deming. 2015. "Oklahoma Monthly Climate Summary for June 2015." http://climate.ok.gov/index.php/climate/summary/reports_summaries

Mesinger, F, G DiMego, E Kalnay, K Mitchell, PC Shafran, W Ebisuzaki, D Jovic, J Woollen, E Rogers, EH Berbery, MB Ek, Y Fan, R Grumbine, W Higgins, H Li, Y Lin, G Manikin, D Parrish, and W Shi. 2006. "North American regional reanalysis." *Bulletin of the American Meteorological Society* 87: 343-360, doi:10.1175/BAMS-87-3-343.

National Centers for Environmental Prediction. 2015. "State of the Climate: Hurricanes and Tropical Storms for June 2015." http://www.ncdc.noaa.gov/sotc/tropical-cyclones/201506

National Hurricane Center. 2015. "National Hurricane Center Tropical Cyclone Report: Tropical Storm Bill," 31 pp. http://www.nhc.noaa.gov/data/tcr/AL022015_Bill.pdf

Rife, DL, JO Pinto, AJ Monaghan, CA Davis, and JR Hannan. 2010. "Global distribution and characteristics of diurnally varying low-level jets." *Journal of Climate* 23: 5041-5064, doi:10.1175/2010JCLI3514.1.

Roundy, JK, CR Ferguson, and EF Wood. 2013. "Temporal variability of land-atmosphere coupling and its implications for drought over the southeast United States." *Journal of Hydrometeorology* 14: 622-635, doi:10.1175/JHM-D-12-090.1.

Santanello, JA, CD Peters-Lidard, SV Kumar, C Alonge, and WK Tao. 2009. "A modeling and observational framework for diagnosing local land-atmosphere coupling on diurnal time scales." *Journal of Hydrometeorol*ogy10: 577-599, doi:10.1175/2009JHM1066.1.

Santanello, JA, C Ferguson, M Ek, P Dirmeyer, O Tuinenburg, C Jacobs, C van Heerwaarden, K Findell, P Gentine, and B Lintner. 2011. "Local land-atmosphere coupling (LoCo) research: Status and results." *GEWEX Newsletter* 21(4): 7-9, http://www.gewex.org/gewex-content/files_mf/1432209597Nov2011.pdf

Seibert, P. F Beyrich, SE Gryning, S Joffre, A Rasmussen, and P Tercier. 2000. "Review and intercomparison of operational methods for the determination of the mixing height." *Atmospheric Environment* 34(7): 1001-1027, doi:10.1016/S1352-2310(99)00349-0.

Sivaraman, C, SA McFarlane, E Chapman, M Jensen, T Toto, S Liu, and M Fischer. 2013. DOE/SC-ARM/TR-132: Planetary Boundary Layer (PBL) Height Value Added Product (VAP): Radiosonde Retrievals, https://www.arm.gov/publications/tech_reports/doe-sc-arm-tr-132.pdf?id=899. 36.

Song, H.J, CR Ferguson, and JK Roundy. 2016. "Land–atmosphere coupling at the Southern Great Plains Atmospheric Radiation Measurement (ARM) field site and its role in anomalous afternoon peak precipitation." *Journal of Hydrometeorology* 17: 541-556, doi:10.1175/JHM-D-15-0045.1.

Stommel, H. 1947. "Entrainment of air into a cumulus cloud." *Journal of Meteorology* 4: 91-94, doi:10.1175/1520-0469(1947))004-0091:EOAIAC>2.0.CO;2.

Turner, DD, and U Lohnert. 2014. "Information content and uncertainties in thermodynamic profiles and liquid cloud properties retrieved from the ground-based Atmospheric Emitted Radiance Interferometer (AERI)." *Journal of Applied Meteorology and Climatology* 53: 752-771, doi:10.1175/JAMC-D-13-0126.1.

TWC, 2015: The Weather Channel: Hurricane News: Tropical Storm Bill leaves behind flooding in central U.S., https://weather.com/storms/hurricane/news/tropical-storm-bill-flooding-heavy-rain-threat

Xia, YL, K Mitchell, M Ek, B Cosgrove, J Sheffield, L Luo, C Alonge, H Wei, J Meng, B Livneh, Q Duan, and D Lohmann. 2012a: "Continental-scale water and energy flux analysis and validation for North American Land Data Assimilation System project phase 2 (NLDAS-2): 2. Validation of model-simulated streamflow." *Journal of Geophysical Research-Atmospheres* 117: D3, doi:10.1029/2011JD016051.

Xia, YL, K Mitchell, M Ek, J Sheffield, B Cosgrove, E Wood, L Luo, C Alonge, H Wei, J Meng, B Livneh, D Lettenmaier, V Koren, Q Duan, KI Mo, Y Fan, and D Mocko. 2012b. "Continental-scale water and energy flux analysis and validation for the North American Land Data Assimilation System project phase 2 (NLDAS-2): 1. Intercomparison and application of model products." *Journal of Geophysical Research-Atmospheres* 117: D3, doi:10.1029/2011JD016048.

Zhang, Y, Z Gao, D Li, Y Li, N Zhang, X Zhao, and J Chen. 2014. "On the computation of planetary boundary-layer height using the bulk Richardson number method." *Geoscientific Model Development* 7: 2599-2611, doi:10.5194/gmd-7-2599-2014.

www.arm.gov

U.S. DEPARTMENT OF
ENERGY

Office of Science